International Journal of Pharmaceutics 683 (2025) 126010

Contents lists available at ScienceDirect

International Journal of Pharmaceutics

journal homepage: www.elsevier.com/locate/ijpharm

Liposomal delivery of a disulfiram metabolite drives copper-mediated tumor immunity

Devon Heroux [a,b], Ada W.Y. Leung [a], Roger Gilabert-Oriol [a], Jayesh Kulkarni [c,d], Malathi Anantha [a], Pieter R. Cullis [c,d], Marcel B. Bally [a,b,e,f,*]

[a] Basic and Translational Research, BC Cancer Research Institute, Vancouver, BC, Canada
[b] Faculty of Medicine, University of British Columbia, Vancouver, BC, Canada
[c] Centre for Molecular Medicine and Therapeutics, Department of Medical Genetics, BC Children's Hospital Research Institute, University of British Columbia, Vancouver, BC, Canada
[d] Department of Biochemistry and Molecular Biology, University of British Columbia, Vancouver, BC, Canada
[e] Department of Pathology and Laboratory Medicine, University of British Columbia, Vancouver, BC, Canada
[f] Department of Pharmaceutical Sciences, University of British Columbia, Vancouver, BC, Canada

ARTICLE INFO

Keywords:
Disulfiram
Copper Diethyldithiocarbamate (DDC)
Liposomes
Immunogenic Cell Death (ICD)
Immunotherapy

ABSTRACT

Disulfiram, traditionally used as an alcohol-aversion drug, has demonstrated anticancer properties attributed to its metabolism into diethyldithiocarbamate (DDC), a potent copper-binding agent. Previously, we developed a liposomal formulation of copper diethyldithiocarbamate ($Cu(DDC)_2$) by incorporating DDC into copper-containing liposomes. In this study, we present an improved formulation achieved by directly mixing DDC and copper in a suspension of empty liposomes, leveraging DDC's copper ionophore-like activity. This method minimizes $Cu(DDC)_2$ precipitation outside the liposomes and enables efficient drug loading at defined molar ratios. The formulation effectively slowed the growth of subcutaneous MDA-MB-231 tumors in mice and showed increased efficacy in 4T1 tumors in immunocompetent mice compared to immunocompromised counterparts. *In vitro*, $Cu(DDC)_2$-treated cancer cells exhibited upregulation of damage-associated molecular patterns (DAMPs), including ATP release, HMGB1 secretion, and calreticulin exposure. Transcriptomic analysis revealed increased expression of immune activation and copper transport genes, further supporting the potential for immunogenic cell death (ICD) induction. In a prophylactic tumor vaccination model, inoculation with $Cu(DDC)_2$-treated CT26 cells delayed tumor growth and conferred protection in a subset of animals, indicating the induction of an adaptive immune response consistent with ICD. These findings align with previous reports of disulfiram-induced ICD and provide functional validation linking this activity to DDC's role as a copper ionophore. This formulation offers a robust and scalable platform for exploring the role of copper as an immune modulator and lays the groundwork for future optimization toward clinical application.

1. Introduction

Disulfiram was approved by the FDA under the brand name Antabuse for treatment of alcohol abuse in 1951. However, for over 50 years, evidence has supported its potential as an anti-cancer agent (Schirmer and Scott, 1966; Wattenberg, 1975). Since the first report of a complete remission in a woman with metastatic breast cancer, several phase I/II trials have been conducted in patients with breast, lung, germ cell, and brain cancers (Dufour et al., 1993; B, M., n.d.; Nechushtan et al., 2015; Mardiak, n.d.). These studies, however, suggest that disulfiram offers limited or no clinical benefit in these settings. This may be due to several factors, including its rapid elimination following oral administration

Abbreviations: FDA, The Food and Drug Administration; DDC, diethyldithiocarbamate; $Cu(DDC)_2$, copper diethydithiocarbamate; Me-DDC, diethyldithiomethylcarbamate; Me-DTC, diethylthiomethylcarbamate; DSF, disulfiram; Cu-i, copper inside liposome; Cu-o, copper outside liposome; CHE, ^{3}[H]-Cholesteryl Hexadecyl Ether; DSPC, 1,2-Distearoyl-*sn*-Glycero-3-Phosphocoline; IC_{50}, inhibitory concentration of 50%; MTD, maximum tolerated dose; i.p., intraperitoneal; i.v., intravenous; SEM, standard error of the mean; TFF, tangential flow filtration; ATP, adenosine triphosphate; HMGB1, high mobility group box 1; CRT, calreticulin; DAMP, damage-associated molecular patterns.

* Corresponding author at: Basic and Translational Research, BC Cancer Research Institute, Vancouver, BC, Canada.
E-mail address: mbally@bccrc.ca (M.B. Bally).

https://doi.org/10.1016/j.ijpharm.2025.126010
Received 26 May 2025; Received in revised form 13 July 2025; Accepted 27 July 2025
Available online 2 August 2025

and evidence that copper (Cu) is required for activity (Viola-Rhenals, 2018). To address the issue of rapid elimination, various formulations have been developed to alter disulfiram's pharmacokinetics and biodistribution, including liposomes, micelles, and PLGA-based systems (Huo et al., 2017; Liu et al., 2014; Fasehee et al., 2016). Notably, many of these formulation efforts did not directly consider the role of copper in disulfiram's anti-cancer activity.

Disulfiram is rapidly metabolized into diethyldithiocarbamate (DDC) and, when mixed with copper, DDC forms $Cu(DDC)_2$ complexes. It is argued that $Cu(DDC)_2$ is the active agent that can kill cancer cells, exhibiting significant activity at doses less than 100 nM *in vitro*. Studies suggest that $Cu(DDC)_2$ is a non-specific agent and its therapeutic potential for treatment of cancer may be due to a number of actions including inhibition of the proteosome (Cvek et al., 2008; Lövborg et al., 2006), NF-kB (Lövborg et al., 2006), and multidrug resistance proteins such as p-glycoprotein (Loo and Clarke, 2000). In addition, DDC has been suggested to transport copper into cells (Helsel and Franz, 2015). Intracellular copper can exert various effects, including free radical scavenging, regulation of the electron transport chain (Hordyjewska et al., 2014), and modulation of immune responses through cytokine production and immune cell activity (Hordyjewska et al., 2014; Lichtnekert et al., 2013).

In our view, and that of others, $Cu(DDC)_2$ is the potentially interesting anticancer agent. However, the $Cu(DDC)_2$ complex is water insoluble and therefore challenging to develop as a therapeutic agent. Efforts to prepare formulations of $Cu(DDC)_2$ suitable for parenteral administration have been described by our group (Wehbe et al., 2017) and others (Paun et al., 2022; Skrott et al., 2017; Kang et al., 2023). The liposomal formulation previously described by our group formulated $Cu(DDC)_2$ by the addition of DDC to copper-containing liposomes. DDC was membrane-permeable, and when it diffused into the liposomes it would complex with copper, precipitate, and become trapped. The apparent solubility of $Cu(DDC)_2$ was increased substantially using this method although precipitation during the preparation of the formulation sometimes interfered with sterile-filtration. More recently, an alternative formulation of $Cu(DDC)_2$ was described where bovine serum albumin (BSA) was present during $Cu(DDC)_2$ formation (Skrott et al., 2017). Specifically, these investigators used a step-wise addition of DDC and copper chloride ($CuCl_2$) in the presence of BSA. This formulation was shown to be effective in breast cancer models.

In the current study, we describe a new liposomal $Cu(DDC)_2$ formulation amenable to large-scale production, using a sequential addition method where DDC and copper sulfate ($CuSO_4$) are added to copper-free liposomes. We present evidence that DDC functions as a copper ionophore, facilitating copper transport into both liposomes and cultured cells. When tested in vivo, the formulation showed greater activity in immunocompetent breast cancer models compared to the same tumors in immunodeficient mice. Additional data suggest that $Cu(DDC)_2$ induces immunogenic cell death (ICD) (Sun et al., 2020; You et al., 2019), a form of cell death that promotes the release of DAMPs and triggers an adaptive immune response against tumors. These results provide proof-of-concept for using ionophore-like small molecules to facilitate controlled *in vitro* and *in vivo* evaluation of copper's biological effects. Together, these results support the use of this strategy as a flexible platform for investigating the immunological and ionophore-driven effects of copper-based therapeutics.

2. Materials and methods

2.1. Materials

^{3}[H]-cholesteryl hexadecyl ether (CHE) and picofluor-15 scintillation fluid were purchased from PerkinElmer, Inc. (Boston, MA). Roswell Park Memorial Institute (RPMI) 1640 medium, Dulbecco's Modified Eagle's Medium (DMEM), Eagle's Minimum Essential Medium (EMEM), Ham's F-12 medium, 0.25 % (w/v) trypsin-EDTA, Hank's balanced salt solution (HBSS) without calcium and magnesium, primary antibody against CRT (product number PA3-900), secondary antibody conjugated to DyLight® 488 (product number 35552), Hoechst 33342 and CellMask™ Deep Red were obtained from Thermo Fisher Scientific (Waltham, MA, USA). Fetal bovine serum (FBS) and l-glutamine (Life Technologies) were obtained from Life Technologies (Carlsbad, CA). Ethidium homodimer-I was obtained from Biotium (Fremont, CA, USA.) Sucrose and chloroform were obtained from EMD Chemicals Inc. (Gibbstown, NJ). 1,2-Distearoyl-*sn*-glycero-3-phosphocholine (DSPC), cholesterol (Chol), sodium diethyldithiocarbamate trihydrate and all other chemicals were purchased from Sigma-Aldrich (Oakville, ON, Canada) as analytical grade reagents.

2.2. Atomic absorption spectroscopy

Concentrations of copper in plasma and tumour homogenates were measured by flameless AAS. Samples were diluted in 0.1 % nitric acid and analyzed using the AAnalyst 600 Atomic Absorption Spectrometer (Perkin Elmer Life Sciences, Waltham, MA). Briefly, samples were dried at 110 °C for 30 s, heated (45 s) to 130 °C, ashed at 1200 °C for 30 s, and atomized and cleaned at 2000 °C (5 s) and 2450 °C (4 s), respectively. The standard curve was generated with 0.1 % nitric acid containing 0, 25, 50, 75, and 100 ng/ml Cu solution.

2.3. HPLC analysis

$Cu(DDC)_2$ concentrations for plasma samples were determined with high-performance liquid chromatography (HPLC; Waters, Milford, MA) at an absorbance wavelength of 435 nm. Plasma samples were mixed with chilled 3 % acidified (glacial acetic acid) methanol, and the samples were centrifuged at 14,000 rpm for 15 min at 4 °C to remove precipitated plasma proteins. Then 20 µL of the supernatant was injected into a Luna Omega 3 µm C18 (2) 100 A (150 × 4.6 mm) column and C18 Symmetry shield guard column (Waters, Mississauga, ON, CA). The mobile phase consisted of 12 % mobile phase "A" (water) and 88 % mobile phase "B" (100 % methanol), with a flow rate of 1 ml/min. Standard curves (ranged from 0.1 µg/mL to 4 µg/mL) were prepared where 3 % acidified methanol was used as the dilution solvent. All standards and samples were kept at 4 °C prior to injections and the column temperature was set to 40 °C.

2.4. Liposome preparation

For DSPC/Chol liposomes, the lipids were first weighed and dissolved in chloroform to achieve a 55:45 (DSPC:Chol) mol:mol ratio. ^{3}[H]-CHE was added as a liposomal lipid marker prior to drying. Specific activity (approximately 20,000–25,000 DPM/µmol total lipid) was then determined by adding 10 µL of the sample to a vial, removing the chloroform and then adding 5 mL of picofluor scintillation fluid. All samples were measured in quadruplicate. The radioactivity was measured on a Packard 1900 TR Liquid Scintillation analyzer. For the bulk sample, chloroform was removed by drying with a stream of nitrogen gas until the samples became thick and syrup-like. To completely remove the chloroform, the samples were then placed under vacuum for at least 3 h, resulting in the formation of a bubbly lipid film. The dried lipid film was then hydrated in various solutions (300 mM copper sulfate; 300 mM citric acid (pH 3.5); 150 mM NaCl, 20 mM citric acid, 20 mM MES, 20 mM HEPES at pH 3.5, pH 5.5, or pH 7.5; sucrose HEPES (SH) pH 7.5 (300 mM sucrose, 20 mM HEPES), HEPES buffered saline (HBS) pH 7.5 (150 mM NaCl, 20 mM HEPES); 1 mL solution per 50 µmol of lipids. The sample was hydrated at 65 °C with constant stirring. The resulting multilamellar liposomes were then extruded fifteen times through two stacked 0.08 µm filters in a 10 mL or 100 mL thermobarrel extruder (LIPEX® Extruder, Evonik Industries, Vancouver, BC, Canada) at 65 °C. The resultant unilamellar liposomes had a mean diameter of approximately 100 ± 20 nm as determined by dynamic light scattering

(ZetaPALS, Brookhaven Instruments Corp., Holtsville, NY). For copper-containing liposomes, the extruded liposomes were passed through a Sephadex G50 column pre-equilibrated with sucrose/HEPES/EDTA (SHE) buffer pH 7.4 (300 mM sucrose, 20 mM HEPES, 15 mM EDTA) to remove unencapsulated copper. The external SHE buffer was further exchanged with the desired external buffers through Sephadex chromatography where the matrix was pre-equilibrated with the desired buffer. The external buffers used in these studies include sucrose HEPES (SH) pH 7.5 (300 mM sucrose, 20 mM HEPES); HEPES buffered saline (HBS) pH 7.5 (150 mM NaCl, 20 mM HEPES); and 150 mM NaCl, 20 mM citric acid, 20 mM MES, 20 mM HEPES at pH 3.5, pH 5.5, or pH 7.5. The final lipid concentration was determined by measuring ^{3}[H]-CHE using liquid scintillation counting.

2.5. Characterization of liposomal Cu(DDC)$_2$

Diethyldithiocarbamate (DDC) and $CuSO_4$ were added step-wise to DSPC/Chol liposomes at drug-to-lipid ratios of 0.1 to 0.4 (mol/mol). The mixture was then continuously mixed with a mini stir-bar in water baths at temperatures of 4 °C and 25 °C. 80 μL aliquots from the Cu(DDC)$_2$-liposome mixture were then taken at various time points (5, 15, 30) and centrifuged through 1 mL Sephadex G-50 mini-spin columns (680 × g for 3 min) to separate the unencapsulated DDC from liposome-associated DDC. For filtration studies, the samples were passed through 0.2 μm filters (Pall Corporation, New York City, NY). Cu(DDC)$_2$ concentrations in the liposomes were determined by measuring absorbance at 435 nm on the Hewlett Packard/Agilent 8453 G1103A UV–Visible Spectrophotometer (Agilent Technologies, Santa Clara, CA, USA) and the liposomal lipid concentrations were measured by liquid scintillation counting. Samples visualized on the UV–visible spectrophotometer were diluted in 100 % HPLC-grade methanol. Morphological characteristics (size, lamellarity, drug loading) of liposome formulations were investigated by CryoTEM as described previously (Renoux and Mrelmljgpbjmlabfoja, 1983). In brief, liposome formulations were concentrated to a liposomal lipid concentration of ~25 μmoles/mL, deposited onto glow-discharged copper grids, and vitrified using a FEI Mark IV Vitrobot (FEI, Hillsboro, OR). CryoTEM imaging was performed using a 200 kV Glacios microscope equipped with a Falcon III camera at the UBC High-Resolution Macromolecular Cryo-Electron Microscopy facility (Vancouver, BC).

2.6. Tissue culture studies

All cell lines were maintained in their respective media supplemented with 10 % FBS and 2 mM L-glutamine. MDA-MB-231 human breast adenocarcinoma cells were obtained from American Type Culture Collection (ATCC) (Manassas, VA, USA) (Cat # HTB-26) and were cultured in RPMI 1640 medium. 4T1 (BALB/cfC3H mammary gland tumour) mouse cells were obtained from ATCC (Cat # CRL-2539), and were cultured in DMEM medium. A2780cp (cisplatin-resistant human ovarian carcinoma cell line) cells was a gift from Mark W. Nachtigal (Univ. of Manitoba, MA, CA) and was cultured in DMEM:F12 medium. DU145 human prostate carcinoma cells were obtained from ATCC (Cat # HTB-81) and were cultured in EMEM medium. LNCaP human prostate carcinoma cells were obtained from ATCC (Cat # CRL-1740), and were cultured in RPMI 1640 medium. JIMT-1 (Herceptin-resistant human breast carcinoma) cells line were obtained from German Collection of Microorganisms and Cell Cultures (DSMZ) (Brunswick, NI, Germany) and were cultured in Ham's F-12/DMEM medium. CT26 murine colon carcinoma cells were obtained from ATCC (CRL-2638) and were cultured in RPMI 1640 medium. All cells were grown and maintained in a humidified incubator at 37 °C and 5 % CO_2. When cells reached 90 % confluence, cells were washed with HBSS without calcium and magnesium, detached with 0.25 % (w/v) trypsin-EDTA and passaged into a new cell culture flask. Cells were subcultured at a ratio of 1:4–1:10 depending on the desired cell density.

MDA-MB-231, JIMT1, DU145 and LNCaP (2000 cells/well) and A2780CP (1500 cells/well) were seeded in a 384-well black-walled, clear bottom plate (Greiner Bio-One, Monroe, NC, USA) in a volume of 50 μL/well and treated the following day. At 72 h post-treatment, cells were stained with 4.87 μM Hoechst 33342 (Life Technologies, Carlsbad, CA) and 312.5 nM ethidium homodimer I (Biotium, Hayward, CA) for viable cells (Hoechst-positive/ethidium homodimer-negative) and dead cells lacking membrane integrity (Hoechst-positive/ethidium homodimer-positive). The cells were incubated with the dyes for 20 min at 37 °C, 5 % CO_2 and then imaged using an IN Cell Analyzer 2200 (GE Healthcare, Mississauga, ON). Cell counts were determined using the Developer Toolbox 1.9 software (GE Healthcare), and percentages of viable cells were normalized to vehicle controls and expressed as fraction affected. All data are plotted using Prism 9.0 (GraphPad Software Inc., La Jolla, CA).

2.7. Copper internalization assay

MDA-MB-231 cells (1×10^6) were seeded in 6 well plates and treated the following day. At 24 h post-treatment, cells were detached with Trypsin/EDTA solution (0.25 % trypsin with EDTA 4Na), and were analyzed for protein concentration with Pierce™ BCA Protein Assay Kit (Thermo Scientific), and copper concentration using AAS as described above. The copper concentration was normalized as nmol copper per mg protein.

2.8. In vitro characterization of immunogenic cell death

For the determination of ATP secretion, CT26 cells (200,000 cells/well) were seeded in a 24-well plate (Corning catalog number 353047) in 300 μL/well of medium. Cells were allowed to attach and grow for 24 h before 100 μL/well of drugs or medium (untreated controls) was added. Cells were incubated with drugs for 24 h and caution was taken not to agitate plates during the experiment to avoid any possible mechanically-stimulated ATP release. At the end of the experiment, 50 μL/well of conditioned cell culture medium (cell supernatant) was transferred to a 96-well white-walled, clear bottom plate already containing 50 μL/well of CellTiter-Glo® 2.0 reagent (Promega, Madison, WI, USA). Pipetting was carefully done to avoid touching the bottom of the wells, so that cells remained adhered to the plate surface and only cell supernatant containing the secreted extracellular ATP (but no cells) was transferred to the new plate containing the reagent. To calculate ATP concentrations, a standard curve was prepared by diluting ATP (10–1000 nM) in medium without FBS. The 96-well plate with samples and CellTiter-Glo® 2.0 reagent was shaken for 2 min at room temperature and further incubated for a total of 15 min. The luminescence signal was recorded in arbitrary units with a FLUOstar OPTIMA microplate reader.

To measure the release of HMGB1, CT26 cells were seeded on a 24-well plate in 300 μL/well of medium containing 200,000 cells/well and incubated for 24 h to allow cell attachment and proliferation. Then, 100 μL/well of drug or medium was added to cells and the cells were incubated for a further 24 h. At the end of the incubation, the extracellular concentration of HMGB1 was determined using the commercial HMGB1 enzyme-linked immunosorbent assay (ELISA) kit (IBL International, catalog number ST51011, Hamburg, Germany). Briefly, 5 μL/well of conditioned cell culture medium was transferred to a pre-coated HMGB1 ELISA 96-well plate containing 105 μL/well of diluent buffer. Care was taken during pipetting to avoid touching the bottom of the well and cell supernatant (with no cells) was transferred to the HMGB1 ELISA 96-well plate. Alternatively, 10 μL/well of diluent buffer, standards or positive control (provided with the commercial kit) were added to wells containing 100 μL/well of diluent buffer. The 96-well plate was shaken for 30 s and incubated for 24 h at 37 °C. The addition of the detection antibody and final detection reaction steps were done following the manufacturer's instructions. The colorimetric signal was determined by

measuring the absorbance at 450 nm (reference wavelength at 600 nm) with a Multiskan® Spectrum microplate reader (Thermo Fisher Scientific). To calculate the concentration of HMGB1, absorbance values were referred to the internal HMGB1 standard curve (range of 2.5–80 ng/mL).

To quantify CRT exposed on the cell membranes, a 96-well black-walled, clear bottom plate was coated with 50 μL/well of 25 μg/mL poly-D-lysine in water for 1 h at room temperature to facilitate cell adherence. The coating solution was aspirated and 20,000 CT26 cells/well were seeded in 100 μL/well. Cells were grown for 24 h and thereafter 100 μL of drugs or medium was added to each well. The cells were exposed to the drugs for 24 h, at which time the cells were washed 3x with 100 μL/well of HBSS with calcium and magnesium without phenol red and fixed with 50 μL/well of 4 % methanol-free formaldehyde diluted in phosphate-buffered saline (PBS) for 20 min at room temperature. Methanol-free formaldehyde was used to minimize permeabilization of cell membranes during fixation. Cells were washed 3x with HBSS and then 50 μL/well of primary antibody against CRT (diluted 1:200 in staining buffer) was added for 1 h on ice. Cells were washed 3x with HBSS and stained with 50 μL/well of secondary antibody conjugated to DyLight® 488 (diluted 1:500 in staining buffer) for 30 min on ice and in the dark. The plate was washed 3x with HBSS and 50 μL/well of Hoechst 33342 (diluted 1:2000 in PBS) and CellMask™ Deep Red (diluted 1:1000) was added for 20 min at room temperature to stain the cell nuclei. Cells were finally washed 3x with HBSS and imaged in 100 μL/well of PBS with the IN Cell Analyzer 2200. Twenty images were acquired for each well. The flat field correction was applied during the image acquisition. Mean fluorescence intensity of CRT on the cell membranes was quantified for each individual cells by conducting a multi-target analysis with the IN Cell 2200 Workstation 3.7 software (GE Healthcare). The average of mean fluorescence intensities for all cells under the same condition was calculated and related to untreated cells in order to express the results as fold-increase in CRT exposure.

2.9. In vivo characterization of $Cu(DDC)_2$

In vivo experiments were conducted using female (NOD)-Rag1^{null}-IL2rγ^{null} (NRG) mice (for tolerability, efficacy, and pharmacokinetics studies), and BALB/c (for efficacy studies) from the Animal Resource Centre (ARC) at the BC Cancer Research Institute (Vancouver, BC, Canada) and were maintained in a pathogen-free environment, housed in groups of four. Mice were housed in microisolators with temperature and humidity monitoring, and were provided enrichment with free access to water and food. All studies adhered to the guidelines of the Canadian Council on Animal Care and were completed under A22-0274 (or previous approved versions), an animal care protocol approved by the Institutional Animal Care Committee (IACC) University of British Columbia. This research team is attempting to meet ARRIVE guidelines (Percie du Sert et al., 2020). The IACC provided regular monitoring of work conducted under this protocol through a post-approval monitoring program.

The $Cu(DDC)_2$ DSPC/Chol liposomes were prepared at a final DDC: total lipid ratio of 0.2 (mol:mol). Prior to administration $Cu(DDC)_2$ DSPC/Chol liposomes, Control "empty" DSPC/Chol liposomes and the $Cu(DDC)_2$ BSA formulation were filter-sterilized through sterile 50 mL vacuum-driven Steriflip filtration system (0.22 μm) Millipore, Billerica, MA, USA). After filtration, the liposomal formulations and BSA formulations were diluted to 0.1 mg $Cu(DDC)_2$/mL for samples injected intraperitoneally (i.p.) at 1 mg/kg, or 0.8 mg $Cu(DDC)_2$/mL for samples injected intravenously (i.v.) at 8 mg/kg. The control liposomes were diluted to match liposomal lipid concentration (175 mg/kg).

To define safe doses of the different $Cu(DDC)_2$ formulations, NRG mice ($n = 3$) were injected i.p. Monday, Tuesday, Wednesday, Thursday, Friday for 2 weeks (M, T, W, Tr, F x2) or injected i.v. (lateral tail vein) for 2 weeks (M, W, F x2). Following injection, the health of the animals was evaluated through monitoring of body weight loss, appetite changes, and other behavioural changes such as lethargy and signs of stress. When signs of severe toxicity were observed, the animals were euthanized (isoflurane overdose followed by CO_2 asphyxiation) for humane reasons. Necropsies were performed on all animals terminated for humane reasons. If the animals survived treatment, they were monitored for 14 days after the administration of the last dose before they were terminated and full necropsies were then completed.

Based on the tolerated dose studies described above, efficacy studies were initiated using the tolerated dose administered to mice bearing established MDA-MB-231 and 4T1 TNBC models. Cells were grown and maintained in media as described above. For *in vivo* studies, cells were harvested from passage #3 to #10 when they reached a confluence of 80–90 %. Cell counts and cell viability were determined using Cellometer Auto T4 (Nexcelom, Lawrence, MA, USA), and cells were then centrifuged at 200 × *g* for 7 min. After removal of supernatant, cells were resuspended in growth medium and inoculation was performed with 10×10^6 cells and 1×10^4 cells for MDA-MB-231 and 4T1 respectively, with subcutaneous injection into the right flank of mice in a volume of 50 μL using a 28-gauge needle. Treatment proceeded once the average tumour volume reached 100 mm^3, and tumour size was determined three times per week by measuring tumour dimensions with callipers starting on first day of treatment. Tumour volumes were calculated based on a formula of (L x W^2)/2, and tumours were allowed to grow to a maximum size of 800 mm^3 before the animals were euthanized for humane reasons. Animals with undetectable tumours by day 25 were excluded.

Pharmacokinetic studies with $Cu(DDC)_2$ formulations were completed in 6–8 weeks old female NRG mice ($n = 4$ per time-point). All mice received a single iv dose (8 mg/kg $Cu(DDC)_2$) prepared in liposomes with the ^{3}[H]-CHE tracer or BSA, and blood was collected *via* cardiac puncture and placed into EDTA coated tubes. The blood was kept on ice and centrifuged (Beckman Coulter Allegra X-15R) at 1500 × *g* for 15 min at 4 °C. Plasma was collected and placed into a separate tube before assaying for copper, $Cu(DDC)_2$, and liposomal-associated [3H]-CHE which were measured with AAS, HPLC, and lipid scintillation counting, respectively.

For the "vaccination" studies CT26 (1×10^6) were seeded in 6-well plates on Day -9, and on Day -8, cells were incubated for 24 h with a concentration of $Cu(DDC)_2$ that would cause 50–70 % cell death after 48 h. At 24 h post treatment (Day -7), cells were detached with fresh enzyme-free cell dissociation buffer (Thermo Fisher, Waltham, MA, USA), the cells were counted and assessed for viability using Cellometer Auto T4. Cells were suspended in phosphate-buffered saline (PBS) at $10x10^6$ cells/mL, and $5x10^5$ cells were inoculated sc (injection volume of 50 μL) into the left flank of mice using a 28-gauge needle. On Day 0, 5×10^5 untreated, parental CT26 cells were injected subcutaneously into the right flank of mice in a volume of 50 μL. Tumour growth in these animals were monitored over time until then animals reached the humane end-point (tumour mass of 800 mg).

2.10. RNA sequencing and transcriptomic analysis

CT26 cells were seeded at 1×10^6 cells/well in 6-well plates and treated with $CuSO_4$ (800 μM), $Cu(DDC)_2$ (1 μM), or vehicle control for 24 h. Total RNA was extracted using the RNeasy Plus Mini Kit (Qiagen), and RNA integrity was confirmed using the Agilent 2100 Bioanalyzer (RIN > 9). Libraries were prepared using the Illumina Stranded mRNA Prep Kit and sequenced on an Illumina NextSeq2000 platform with 59 bp paired-end reads. Sequencing reads were demultiplexed using BCL Convert and aligned to the *Mus musculus* reference genome (mm10) using the DRAGEN RNA pipeline on BaseSpace Sequence Hub. Gene-level count matrices were generated using the DRAGEN Differential Expression App, and differential expression analysis was conducted using DESeq2 (v1.38.3) with default shrinkage estimation for $\log_2$ fold change.

Gene set enrichment analysis (GSEA) was performed on ranked gene lists using the fgsea and clusterProfiler R packages (v4.2.2), referencing

GO Biological Process terms. dot plots, and ridge plots were used to visualize pathway activation across conditions. Changes in immune signaling, copper metabolism, and cell stress responses were examined, including transcript-level shifts in selected genes.

2.11. Statistical analysis

GraphPad Prism 9.0 software was used to plot all data as mean ± standard error of the mean (SEM) as described in the figure legends. In vitro assays were analyzed using unpaired two-tailed t-tests. Tumour growth comparisons were performed using two-way analysis of variance (ANOVA) followed by Tukey's multiple comparisons test. Survival analyses were performed using the log-rank test. Statistical significance is denoted as follows: $P < 0.05$ (*), $P < 0.01$ (**), $P < 0.001$ (***).

3. Results

$Cu(DDC)_2$ may be useful as a therapeutic agent in the treatment of cancer, but is insoluble (Fig. 1H). Our team previously described a formulation for liposomal $Cu(DDC)_2$ where the liposomes were prepared with encapsulated $CuSO_4$ (copper inside; Cu-i) (Fig. 1D-F) (Wehbe et al., 2017; Wehbe et al., 2016); this increased the apparent solubility of Cu $(DDC)_2$ more than 500-fold. Subsequently, Skrott et al (Skrott et al., 2017) described a $Cu(DDC)_2$ formulation using BSA where DDC was added to a copper-containing solution in the presence of BSA (Fig. 1G). No precipitation was noted. To assess whether $Cu(DDC)_2$ remained in solution in the presence of "empty" liposomes, a similar approach was tried. Surprisingly, a liposomal formulation of $Cu(DDC)_2$ could be prepared when DDC and $CuSO_4$ were added sequentially to copper-free liposomes (copper outside; Cu-o) (Fig. 1A-C). This formulation led to the apparent solubilization of $Cu(DDC)_2$, comparable to the Cu-i method. The association of $Cu(DDC)_2$ with liposomes was measured over time at 4 °C and room temperature (RT). In both formulations, $Cu(DDC)_2$ rapidly associated with the liposomes at RT, and a final $Cu(DDC)_2$ to liposomal lipid ratio of ~0.1 was measured after separating the liposomes from unassociated $Cu(DDC)_2$ via a Sephadex G-50 column. The only difference in $Cu(DDC)_2$ association with liposomes was observed when the incubation was done at 4 °C. At this temperature, the rate of Cu $(DDC)_2$ association with the Cu-i method was slower, and complete association was only noted after 30 min. In contrast, when the Cu-o method was used, $Cu(DDC)_2$ association with liposomes peaked at a $Cu(DDC)_2$ to liposomal lipid ratio of ~0.05 (50 % of expected) and there

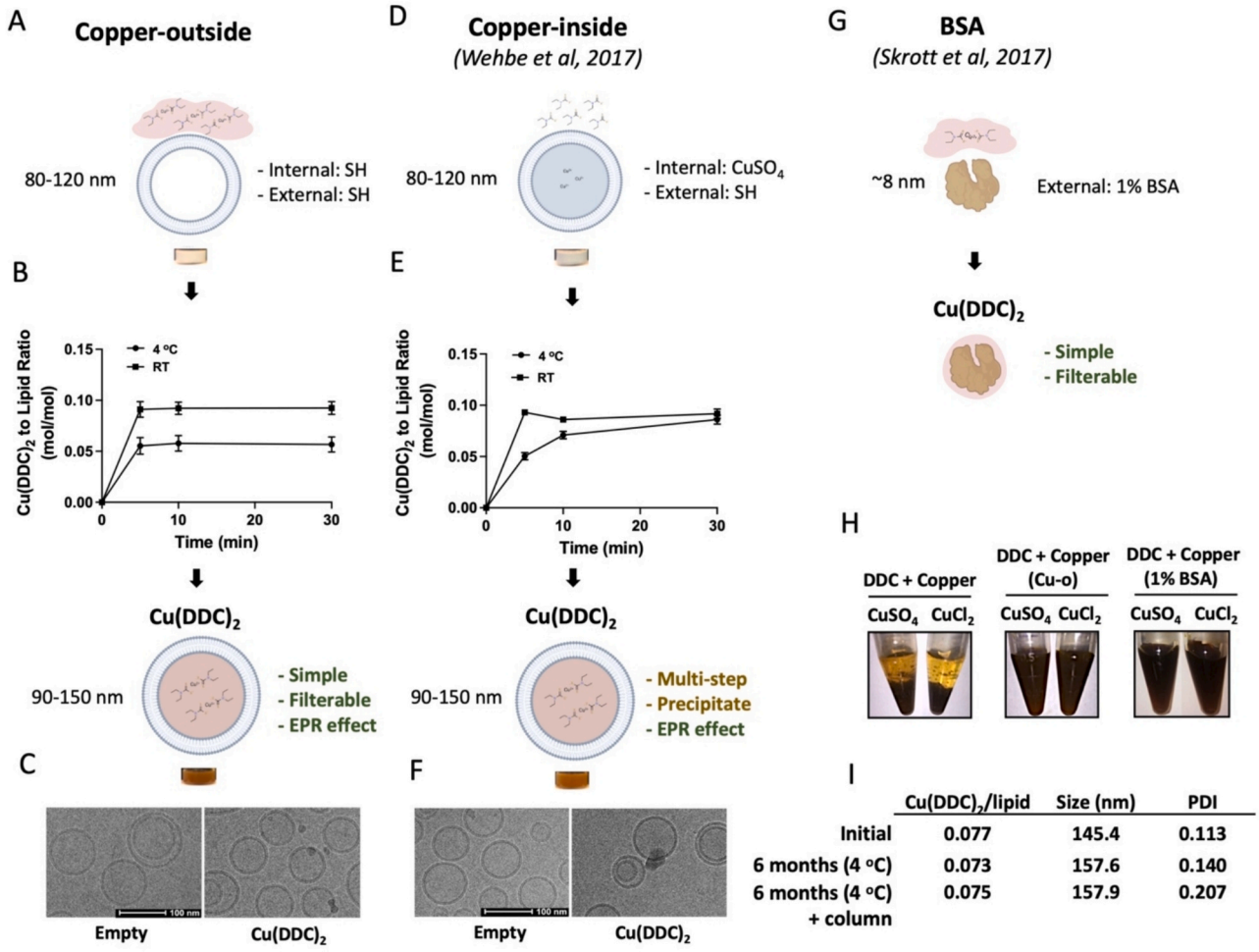

Fig. 1. $Cu(DDC)_2$ formulation and characterization using liposomes and BSA. (A–C) "Copper-outside" (Cu-o) liposomes are prepared by adding 22 mM DDC to $CuSO_4$ (2:1 M ratio) in buffer with 300 mM sucrose HEPES (SH) (pH 7.5), forming $Cu(DDC)_2$ externally, with a $Cu(DDC)_2$-to-lipid ratio of ~0.1 within 5 min at RT. The resulting formulation is simple, filterable, and leverages the enhanced permeability and retention (EPR) effect (green), with diameters of 110–150 nm. (D–F) "Copper-inside" (Cu-i) liposomes are pre-loaded with 300 mM $CuSO_4$ and then incubated with 22 mM DDC externally, with similar loading kinetics as Cu-o at RT. This method also supports EPR-based delivery (green) but requires multiple steps and can produce precipitate, complicating filtration (yellow). (G) BSA-based Cu $(DDC)_2$ (~8 nm) is generated by combining 22 mM DDC with $CuSO_4$ or $CuCl_2$ (2:1 M ratio) in 1 % BSA. This approach is simple and filterable (green) but lacks size-based tumor targeting. (H) Solubility of $Cu(DDC)_2$ formed in water, Cu-o liposomes, or BSA using $CuSO_4$ or $CuCl_2$. (I) Cu-o liposomes remain stable after 6 months at 4 °C, maintaining consistent $Cu(DDC)_2$-to-lipid ratios (~0.075–0.077), size (~145–158 nm), and low PDI values, before and after column purification.

was visible $Cu(DDC)_2$ precipitation. The two formulations prepared at 25 °C were characterized by cryo-TEM (see Methods) and representative photomicrographs are provided in Fig. 1C, F. No electron-dense liposome interior was noted in either formulation and the size and morphology of the two formulations were comparable. Previous studies have used Cu salts including $CuCl_2$ for DDC complexation (Skrott et al., 2017), and for initial formulation assessments, both $CuCl_2$ and $CuSO_4$ were tested for Cu-o and BSA loading efficiency, with similar results observed (Fig. 1H); all subsequent optimization steps were conducted using $CuSO_4$. Cu-o was stable at 6 months during storage at 4 °C, with minimal changes in size or polydispersity (Fig. 1I).

The formulation was evaluated as a function of internal and external buffers by varying buffer compositions and pH. The results have been summarized in Fig. 2. Formation of $Cu(DDC)_2$ is known to be dependent on pH, due in part to the hydrogenation of thiol groups at low pH (Otoniel et al., 2003). We assessed formation of $Cu(DDC)_2$ at pH 3.5, pH 5.5 and pH 7.5 (Fig. 2A) which highlights that $Cu(DDC)_2$ does not form at low pH. For the liposomal formulations (Fig. 2B), the liposomes were prepared with internal buffers containing: (i) citric acid (pH 3.5), (ii) SH (pH 7.5), or (iii) HBS (pH 7.5), and the external buffer consisted of a mixture of citric acid, HEPES, MES, and NaCl (CHMN) to enable good buffering capacity through a pH range of 3.5–7.5. Similar to the results in Fig. 2A, when the liposomes were placed in a pH 3.5 external buffer, little or no $Cu(DDC)_2$ was associated with the liposomes. Under these conditions $Cu(DDC)_2$ formation was not observed. When the external buffer was increased to pH 5.5 or 7.5, $Cu(DDC)_2$ associated with the liposomes even when the trapped internal buffer was pH 3.5. The association of $Cu(DDC)_2$ with liposomes was most efficient when the external pH was 7.5.

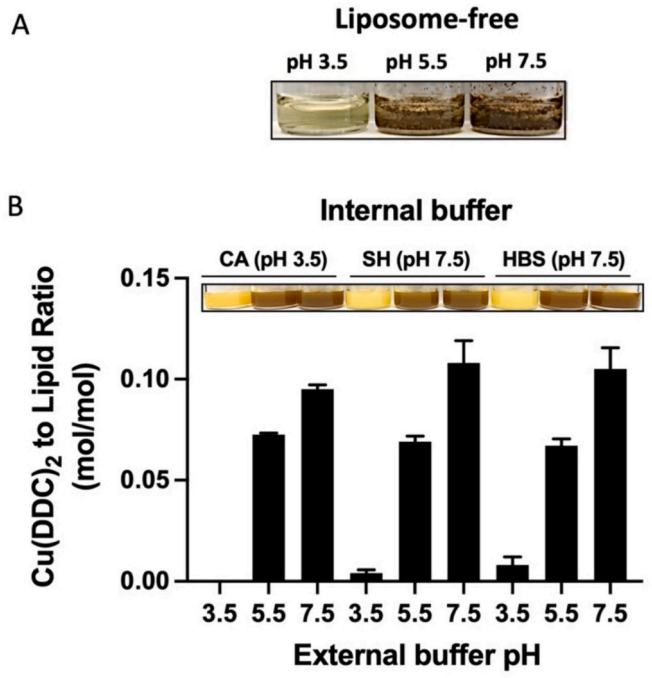

Fig. 2. External buffer with a pH of 7.5 is optimal for $Cu(DDC)_2$ formation. $Cu(DDC)_2$ does not form in pH 3.5 buffer in the absence of liposomes. However, obvious $Cu(DDC)_2$ precipitates form when the buffer used is at pH 5.5 and pH 7.5 (A). $Cu(DDC)_2$ was formulated with liposomes using the Cu-o method when the liposomes were prepared to have an internal buffer of pH 3.5 (300 mM citric acid (CA), pH 7.5 (300 mM sucrose HEPES (SH)) or pH 7.5 (300 mM HEPES-buffered saline (HBS)), with an external buffer of pH 3.5, 5.5, or 7.5 (20 mM HEPES, 20 mM MES, 20 mM citric acid, 150 mM NaCl, adjusted to the specified pH with 1 M NaOH). An aqueous solution of DDC (22 mM was added to the liposomes such that the final DDC to $CuSO_4$ molar ratio was 2:1 (B). After a 30-minute incubation at RT, the liposomes were passed through Sephadex G-50 spin columns to separate un-associated $Cu(DDC)_2$, and the excluded fractions were analyzed; $Cu(DDC)_2$ and liposomal lipid concentrations were measured by UV–Vis spectroscopy and liquid scintillation counting, respectively. Data are plotted as mean ± SEM.

Further characterization of the $Cu(DDC)_2$ liposomes focused on liposomes prepared using an external pH of 7.5 and the efficiency of $Cu(DDC)_2$ association was measured as a function of internal pH. When the internal pH was 3.5, $Cu(DDC)_2$ association with the liposomes was reduced. A maximum $Cu(DDC)_2$ to liposomal lipid ratio of 0.2 was achievable under these conditions. In contrast, as lipid concentration decreased to 1 mM with $Cu(DDC)_2$ levels held constant at 10 mM, $Cu(DDC)_2$ to liposomal lipid molar ratios of approximately 1 were achievable when the internal pH was 7.5; albeit the capacity was greatest when using trapped HBS (pH 7.5) compared to SH (pH 7.5) (Fig. 3A). Although higher $Cu(DDC)_2$ to liposomal lipid ratios could be achieved, the resulting formulations could not be filtered through a 0.22 μm filter, suggesting the presence of precipitated $Cu(DDC)_2$. In fact, the only $Cu(DDC)_2$ to liposomal lipid ratio that could be consistently passed through the sterile filtration filters was 0.1. To determine whether the $Cu(DDC)_2$ was associated with the liposomes, the internal pH 7.5 formulations prepared at $Cu(DDC)_2$ to liposomal lipid molar ratio of 0.1 were fractionated on a Sephadex G-50 column to assess co-elution of $Cu(DDC)_2$ and liposomal lipid (Fig. 3B). If a $Cu(DDC)_2$ precipitate formed, the precipitate would remain at the top of the column (data not shown). When $Cu(DDC)_2$ formed in the presence of liposomes (HBS (Fig. 3B) or SH (Fig. 3C) the $Cu(DDC)_2$ co-eluted with the liposomes.

The conditions used to prepare $Cu(DDC)_2$ liposomes were further characterized as shown in Fig. 4A and B. The results are consistent with the results shown in Fig. 3, and suggest formulations prepared at a fixed liposomal lipid concentration (Fig. 4A) or a fixed $Cu(DDC)_2$ concentration (Fig. 4B) to generate a range of theoretical $Cu(DDC)_2$-to-liposomal lipid ratios (0.05, 0.1, 0.2) could be prepared. There were close associations between the theoretical and actual $Cu(DDC)_2$-to-liposomal lipid ratios regardless of approach. The results verify the 1:2 Cu to DDC ratio, but the 0.2 $Cu(DDC)_2$-to-liposomal lipid ratio formulation could not be sterile filtered (0.22 μm filter).

Other investigators have suggested that DDC can transport copper through cellular membranes (Helsel and Franz, 2015); (Allensworth et al., 2015). It was postulated that the method of internalization in the present liposomal formulation was due to DDC's ionophore-like activity, binding membrane-impermeable charged copper ions and transporting the neutralized complex through the liposomal membrane. To test the copper ionophore-like properties of DDC, DDC was added to liposomes and then excess copper was added. Liposomes prepared with an internal buffer (20 mM HEPES, 20 mM MES, 20 mM citric acid, 150 mM NaCl) (pH of 3.5–7.5) and a pH 7.5 SH external (20 mM liposomal lipid) were mixed with DDC (4 mM) and then $CuSO_4$ (2, 10 mM) and the copper levels in the liposomes were then determined (Fig. 5A). The $Cu(DDC)_2$ to liposomal lipid ratios were maintained at essentially 0.1. However, when high levels of external copper were used (10 mM) all formulations had a higher than predicted copper association. This was most evident when the internal pH was 5.5 and 7.5, where copper to lipid ratios exceeded 0.3.

These studies also evaluated liposomal copper to lipid levels when the concentration of DDC added to the liposomes increased from 2 mM to 8 mM and the concentration of copper was increased from 2 mM to 10 mM. The level of $Cu(DDC)_2$ that became associated with the liposomes could be predicted based on the stoichiometric ratio of the two components (Fig. 5B). However, the level of copper that became associated with the liposomes suggested that there were enhanced copper levels than what would be predicted based on DDC levels (Fig. 5C).

An assessment of DDC-mediated transport of copper into a cell line was completed. MDA-MB-231 cells were selected because subsequent efficacy studies were completed in mice with established sc tumours created following inoculation with this triple-negative breast cancer cell line. The association of copper with these cells was determined at 0.5, 1,

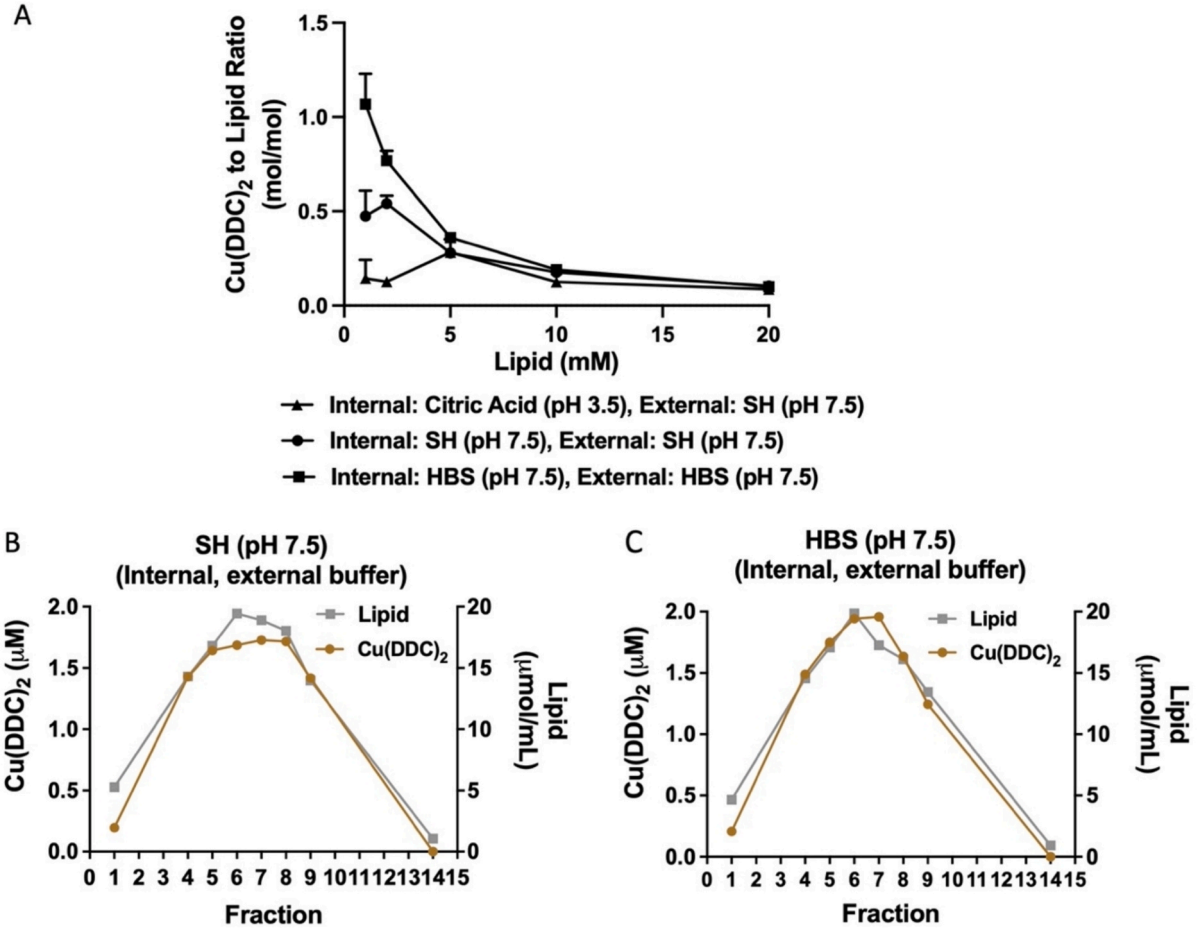

Fig. 3. Internal buffer with pH 7.5 increases the $Cu(DDC)_2$ to liposomal lipid ratio. $Cu(DDC)_2$ was generated in liposomes with various internal buffers (citric acid, pH 3.5; SH or HBS, pH 7.5) and external buffers (SH or HBS, pH 7.5) with limiting concentrations of liposomal lipid to establish capacity of $Cu(DDC)_2$ association with the liposomes (A). After 30 min, samples were passed through spin columns containing Sephadex G-50 beads to separate non-associated $Cu(DDC)_2$. Data are plotted as mean ± SEM. The formulations containing internal/external buffers of SH (B) and HBS (C) were passed through 5 ml Sephadex G-50 columns, and fractions were analyzed for $Cu(DDC)_2$ and liposomal lipid by UV–Vis spectroscopy and liquid scintillation counting.

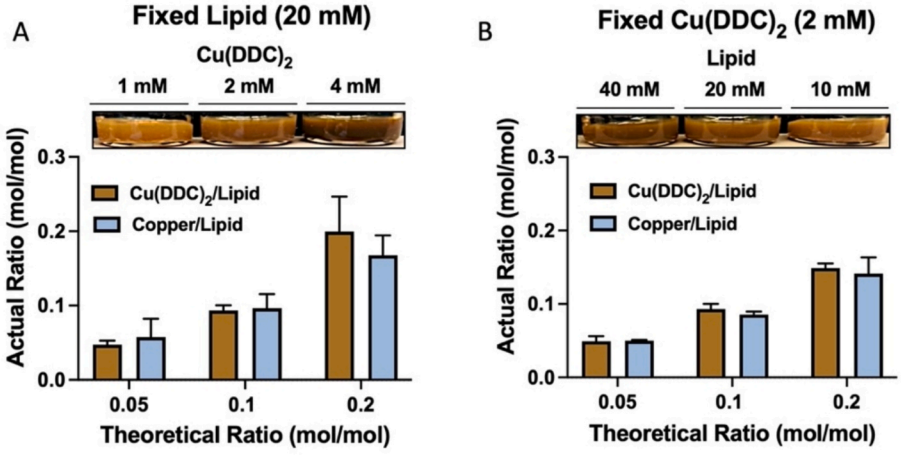

Fig. 4. $Cu(DDC)_2$ association with liposomes while varying the initial $Cu(DDC)_2$ to liposomal lipid ratio. In order to determine the role of $Cu(DDC)_2$ and lipid concentrations in loading efficiency, the $Cu(DDC)_2$ formation was assessed when the liposomal lipid concentration was fixed at 20 mM (A) and while the $Cu(DDC)_2$ was fixed at 2 mM (B). Liposome-associated $Cu(DDC)_2$ and copper were determined by UV–visible spectroscopy and AAS. Liposomal lipid concentration was determined by liquid scintillation counting. Data are plotted as mean ± SEM.

2 and 4 hrs after 5 μM DDC and 2.5 μM copper sulfate were added. The results shown in Fig. 5D, indicate that cell-associated copper levels increased over time. In the absence of DDC or copper there was less than 1 nmole copper per mg cellular protein. In the presence of DDC and copper, the level of copper increased more than 40-fold to levels of 20 nmol copper per mg cellular protein. The uptake of copper into this cell

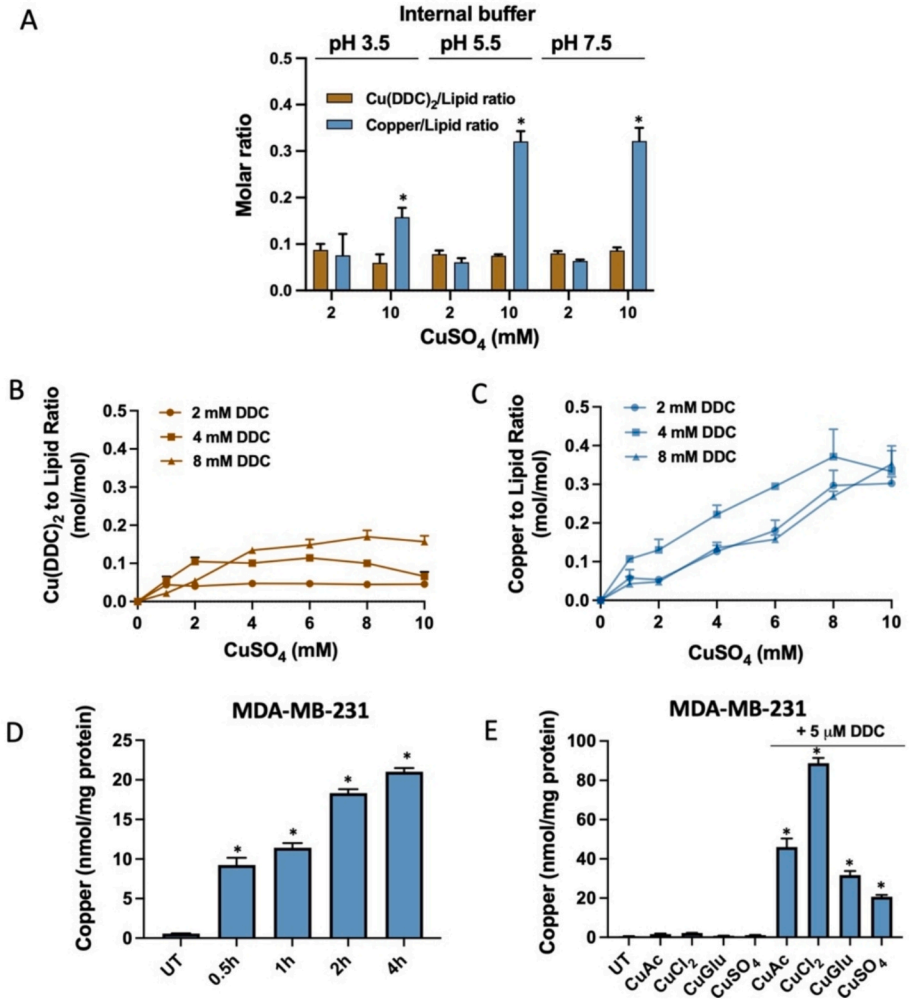

Fig. 5. DDC has copper ionophore-like properties and can move copper across liposomal lipid bilayers as well as cellular membranes. To gain a better understanding of how copper and DDC added to the outside of liposomes resulted in $Cu(DDC)_2$ formation inside the liposomes an evaluation of copper transport was assessed when there was copper excess (relative to the established 2:1 ratio), liposomes containing internal buffers of pH 3.5, 5.5, and 7.5 (20 mM HEPES, 20 mM MES, 20 mM citric acid, 150 mM NaCl), with a SH external buffer (pH 7.5) were mixed with DDC and $CuSO_4$ at the indicated ratios (A). The liposomes were separated on mini-Sephadex G-50 columns and $Cu(DDC)_2$, liposomal lipid and copper were measured with UV–Vis spectroscopy, liquid scintillation counting, and atomic absorption spectroscopy (AAS), respectively. When excess copper was present the copper to liposomal lipid ratio increased while the $Cu(DDC)_2$ to liposomal lipid ratio remained approximately 0.1. When copper was added to liposomes in the absence of DDC no copper became associated with the liposomes. Liposomes were mixed with DDC (2, 4, 8 mM) and $CuSO_4$ (1, 2, 4, 6, 8, 10 mM) and the $Cu(DDC)_2$-to-liposomal lipid ratios (B) and copper-to-lipid ratios (C) were determined. To determine whether addition of copper and DDC to cells in cultures triple-negative breast cancer cells (1×10^6 MDA-MB-231 cells) in T25 flasks were assessed for copper levels after 5 μM DDC and 2.5 μM $CuSO_4$ were added (D). Internal copper was then measured at the times indicated with AAS. Several forms of copper (acetate, chloride, gluconate, sulfate) were also combined with 5 μM DDC, or without DDC (E) and the copper levels in the cells were determined as described in the Methods. Data are plotted as mean ± SEM. *P < 0.05.

line varied depending on the copper salt used (Fig. 5E). In the absence of DDC, the nmole copper per mg cellular protein level was always less than 1.5, but in the presence of DDC, this increased to 20, 30, 42, and 85 nmole copper per mg cellular protein when copper sulfate, copper gluconate, copper acetate and copper chloride were added, respectively.

One goal of this research was to compare the therapeutic activity of the BSA formulation of Cu $Cu(DDC)_2$ (Skrott et al., 2017) to a liposomal formulation of $Cu(DDC)_2$. Studies evaluated liposomal formulations where DDC and copper were added to the outside of liposomes, a method that would be comparable to adding DDC and copper to BSA in solution. Initial studies, summarized in Fig. 6, used cells in culture to assess the cytotoxicity of the BSA and the liposomal $Cu(DDC)_2$ formulations. The dose–response curves used to define the IC_{50} of the formulations (Cu-o, Cu-i, BSA) in MDA-MB-231 cells were identical (Fig. 6A). Using the Cu-o liposomal formulation, it was clear that the dose–response curves were essentially identical regardless of whether the cells were exposed to $Cu(DDC)_2$ for 4 h or 72 h (Fig. 6B). Finally, a comparison of $Cu(DDC)_2$ in DMSO was made using different tumour cell lines originating from breast (JIMT-1, MDA-MB-231), prostate (DU145, LNCap), and lung (A2780CP), and all demonstrated similar potency with IC_{50}'s ranging from 0.05 to 0.13 μM (Fig. 6C).

We compared the pharmacokinetics (PK) of $Cu(DDC)_2$ formulated in liposomes (Cu-o formulation)to $Cu(DDC)_2$ formulated using BSA. The results are summarized in Fig. 7. The maximum tolerated dose (MTD) for both formulations was determined in immunodeficient NRG mice following iv injections on Monday, Wednesday, and Friday for 2 weeks (M, W, F x2) and 8 mg/kg was tolerated and thus used for the PK studies shown in Fig. 7. For these studies, a single iv injection of 8 mg/kg was given to NRG mice, and $Cu(DDC)_2$ and liposomal lipid concentrations in the plasma were determined at the indicated time points. $Cu(DDC)_2$ was rapidly eliminated from the plasma compartment, with approximately 99 % of the $Cu(DDC)_2$ eliminated within 5 min. After 20 min the Cu $(DDC)_2$ level was below detectable limits of the assay used. The area under the curve (AUC) estimations for $Cu(DDC)_2$ following

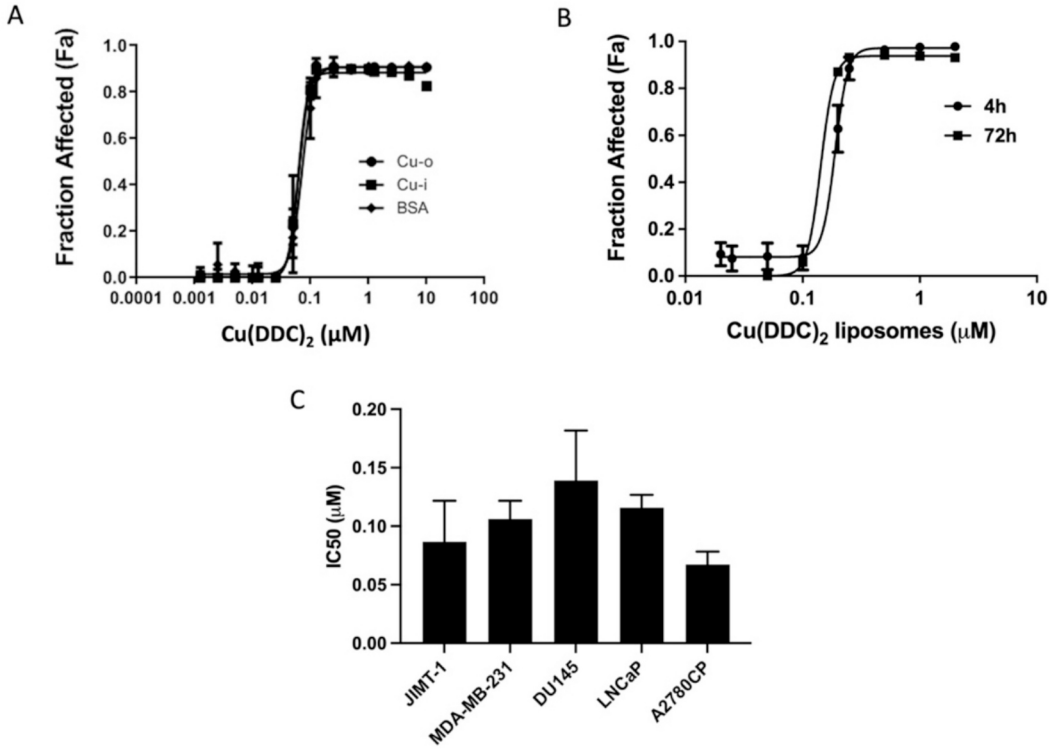

Fig. 6. Cytotoxicity of liposomal and BSA $Cu(DDC)_2$ formulations. Cytotoxic effects of two liposomal $Cu(DDC)_2$ formulations (Cu-i and Cu-o) were compared to $Cu(DDC)_2$ formed in the presence of BSA in MDA-MB-231 cells (A). Cells were stained with Hoechst 33342 and ethidium homodimer I, and imaged and quantified using an IN Cell Analyzer 2200 with percentages of viable cells normalized to vehicle controls and expressed as fraction affected. Cytotoxicity of the liposomal $Cu(DDC)_2$ formulation (Cu-o) was measured after a 4 h and a 72 h exposure time (B). When cells were exposed to $Cu(DDC)_2$ for 4 h, the cells were washed with PBS after 4 h and replenished with media, then imaged after a total of 72 h. The IC50 (72 h exposure time) of the liposomal $Cu(DDC)_2$ formulation (Cu-o) against the MDA-MB-231 cell line was approximately 100 nM. If $Cu(DDC)_2$ was prepared in DMSO the IC50 (72 h) was comparable for JIMT-1 (human breast cancer cell line), MDA-MB-231 (human breast cancer cells), DU145 (prostate cancer cell line), LNCaP (prostate cancer cell line), and A2780CP (a cisplatin-resistant lung cancer cell line) (C). Data points represent the mean ± SEM.

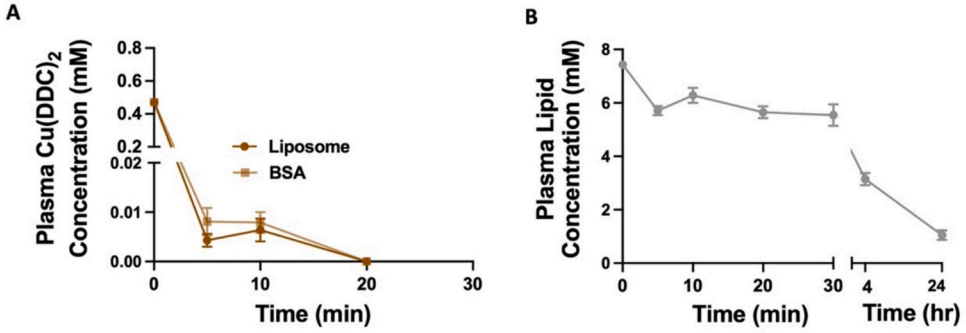

Fig. 7. Liposomal and BSA formulations of $Cu(DDC)_2$ exhibit similar behaviour following intravenous administration in NRG mice. $Cu(DDC)_2$ formulated in liposomes and BSA were injected at a $Cu(DDC)_2$ dose of 8 mg/kg. The level of $Cu(DDC)_2$ in the plasma was measured by HPLC (A), and liposomal lipid was measured by assessing ^{3}H-CHE as a non-exchangeable, non-metabolizable liposomal lipid marker by liquid scintillation counting (B). All data are plotted as mean ± SEM (n = 3–7).

administration of the Cu-o liposomal formulation (7.48 μg-hr/ml) and BSA formulation (7.66 μg-hr/ml) were comparable. The results were comparable to results obtained when measuring the plasma elimination of the Cu-i formulation (Wehbe et al., 2017). It should be noted that >75 % of the injected liposomal lipid dose was present in the plasma compartment 30 min following iv injection and 40 % was remaining 4 h after injection. It can be suggested that both methods provide an effective means to solubilize $Cu(DDC)_2$ and that $Cu(DDC)_2$ dissociates from the liposomes almost immediately following administration, while the liposomes are retained in the plasma compartment for extended time periods.

The anti-tumour efficacy of the Cu-o and BSA $Cu(DDC)_2$ formulations was assessed in a subcutaneous xenograft model of MDA-MB-231. This cell line was chosen, in part, because of the previously reported activity using the BSA $Cu(DDC)_2$ formulations (Skrott et al., 2017). NRG mice with established tumours (≥100 mm^3) were injected iv using a Cu $(DDC)_2$ dose of 8 mg/kg for the Cu-o and BSA formulation. The Cu $(DDC)_2$ formulations were administered on M, W, F x 2 weeks (Fig. 8A). Treatment with these formulations delayed tumour progression. At 35 days there was a 37 % reduction in tumour volume relative to controls for animals treated with the Cu-o liposomal formulation and a 32 % reduction in tumour volume when the mice were treated with the BSA

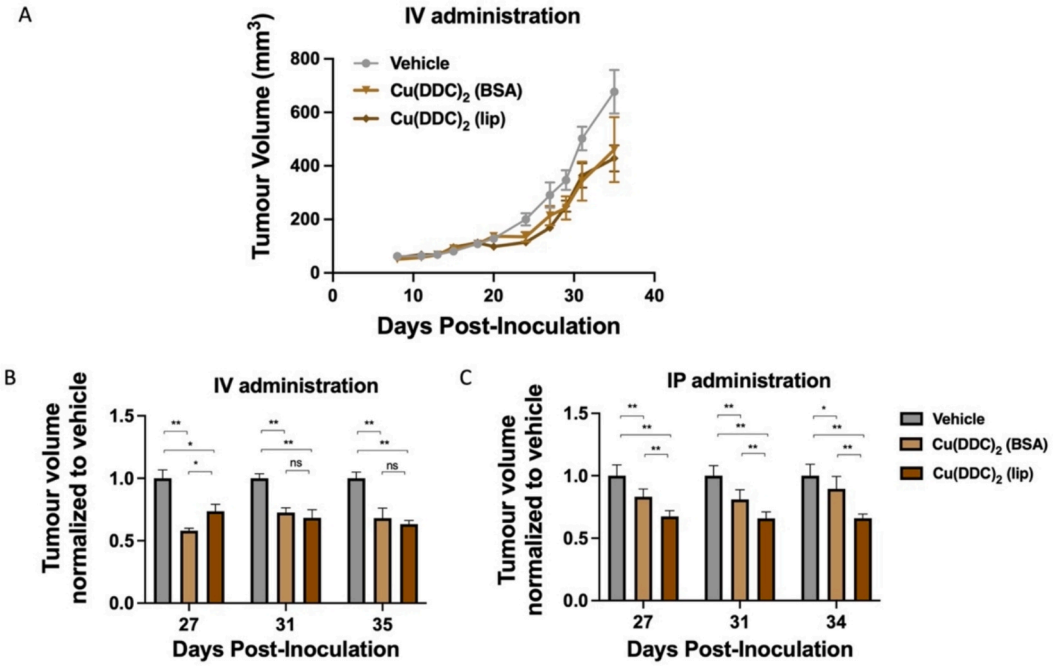

Fig. 8. Efficacy of liposomal and BSA $Cu(DDC)_2$ formulations in a MDA-MB-231 sc xenograft model. Female NRG mice were inoculated subcutaneously with 1×10^7 MDA-MB-231 cells, and tumour-bearing mice ($\geq$100 mm^3) were injected intravenously (IV) (A-B) at a $Cu(DDC)_2$ dose of 8 mg/kg given Monday, Wednesday and Friday for two weeks. The data is plotted as mean ± SEM. For animals given an IP administration, 1 mg/kg $Cu(DDC)_2$ was dosed daily Monday to Friday for two weeks (C). * $P < 0.05$; ** $P < 0.01$.

$Cu(DDC)_2$ formulations. The difference in activity was not significant ($p > 0.05$). At the 8 mg/kg iv dose, several animals developed tail swelling ranging from mild to severe (including one termination-level case), along with occasional coat changes and hyperactivity, but no clinical signs suggestive of systemic or organ-specific toxicity were observed.

The previous study assessing efficacy in MDA-MB-231 tumour-bearing mice was done using ip administration of the drug and the MTD was determined to be 1 mg/kg M-F x 2 as an adaptation of the >30 day dosing schedule used by Skrott et al. (Skrott et al., 2017). This dosing strategy was well tolerated for both formulations with no signs of local irritation of systemic toxicity, and the results have been summarized in Fig. 8C. Thirty-four days following treatment there was a 35 % and 10 % reduction in tumour volume when mice were injected (ip) with the Cu-o $Cu(DDC)_2$ and BSA $Cu(DDC)_2$ formulation, respectively. This was statistically significant ($p < 0.05$) when compared to the vehicle control and between the formulations. The efficacy data obtained for animals treated with the BSA $Cu(DDC)_2$ formulation was less than that reported by Skrott et al. (Skrott et al., 2017) and may be due to changes in the dosing length, injection volume, mice used, cell line used, and/or the animal facility used.

The Cu-o $Cu(DDC)_2$ formulation demonstrated modest efficacy in the immunodeficient NRG MDA-MB-231 sc model but was comparable to the BSA $Cu(DDC)_2$ formulation in a side-by-side comparison in the same model, with a slight improvement in observed following IP administration. There is evidence that disulfiram and/or $Cu(DDC)_2$ has the potential to activate the immune system (Sun et al., 2020; You et al., 2019; Zheng et al., 2021), thus it was important to determine the activity of the $Cu(DDC)_2$ formulation in a syngeneic immune competent model. Focusing on the Cu-o $Cu(DDC)_2$ formulation, the activity of the formulation was determined in mice with established 4T1 (breast carcinoma cell line) tumours. The studies compared the activity when the tumours were established in immune competent mice (Balb/c) or in immune deficient NRG mice. Mice with established tumours (100–150 mm^3) were treated IV with the Cu-o $Cu(DDC)_2$ formulation (8 mg/kg three times every 4 days (q4dx3)). The control groups (untreated (not shown) or dextrose treated) exhibited similar tumour growth rates in the immune competent and immune deficient mice. The Cu-o $Cu(DDC)_2$ formulation did not have a therapeutic effect in NRG mice with established 4T1 tumours. However, when the efficacy study was determined in Balb/c mice with established 4T1 tumours there was a 41 % decrease in tumour volume (Fig. 9A), and at the time when all the NRG mice were euthanized due to tumour progression (tumour volumes > 800 mg) 73 % of the 4T1 tumour bearing Balb/c mice were still alive (Fig. 9B). These results indicate a significant survival advantage in immune competent mice with the 4T1 tumours.

Female immune competent Balb/c and immune comprised Balb/c nu/nu were inoculated subcutaneously with 1×10^4 syngeneic 4T1 cells, and tumour-bearing mice (100–150 mm^3) were injected i.v. with 8 mg/kg $Cu(DDC)_2$ three times at intervals of 4 days (q4dx3). Tumour volumes on day 23 (A) and percentage increase in survival at day 32 (B) are plotted as mean ± SEM ($n = 6$–11). *$P < 0.05$.

The benefits of $Cu(DDC)_2$ in immunocompetent mice prompted investigation into $Cu(DDC)_2$'s potential to induce immunogenic cell death (ICD), a regulated form of cell death that promotes anti-tumor immunity via the release of DAMPs. ICD is marked by early surface exposure of calreticulin (CRT), ATP release during apoptosis, and HMGB1 release during late necrosis, along with inflammatory cytokine signaling.

RNA-seq analysis of CT26 cells treated with $Cu(DDC)_2$ for 24 h showed strong enrichment of pathways linked to apoptosis, oxidative and ER stress, cytokine signaling, and adaptive immunity, while pathways related to cell cycle were inhibited. (Fig. 10A–C). Transcriptional changes included increased expression of *Calr*, *Hmgb1*, *Il1a*, *Tnf*, *Ccl5*, and copper exporters such as *Atp7a*, while *Slc31a1* (CTR1), the primary copper importer, was upregulated with $CuSO_4$ but remained unchanged with $Cu(DDC)_2$ (Fig. 10C). This may reflect differences in copper uptake, as $Cu(DDC)_2$ likely bypasses CTR1 via passive diffusion or direct membrane interaction. Cu has been reported to induce NF-kB response in tumor and immune cells (McElwee et al., 2009; Caetano-Silva et al., 2021), and here while both $CuSO_4$ and $Cu(DDC)_2$ decreased specific pathways related to NF-kB kinase activation, both treatments generally exhibited increased expression in genes and broader pathways

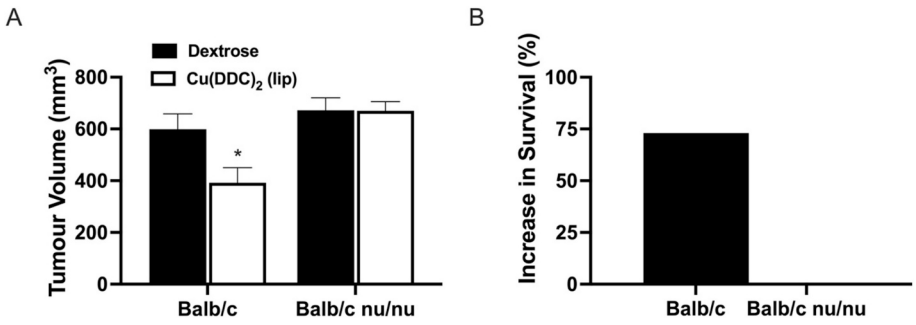

Fig. 9. Liposomal $Cu(DDC)_2$ exhibits enhanced activity in an immunocompetent 4T1 syngeneic xenograft model.

associated with NF-kB activation.

Functional assays confirmed the induction of DAMPs by $Cu(DDC)_2$, including a 7-fold increase in ATP release, a 4-fold increase in HMGB1 secretion, and a 2-fold increase in surface CRT exposure compared to untreated or singly treated controls (Fig. 10D–F). To assess whether this translated to *in vivo* immunogenicity, a prophylactic tumor vaccination model was used. CT26 cells treated *in vitro* with $Cu(DDC)_2$ at a dose inducing ~50 % cell death were injected into the left flank of BALB/c mice, followed by a rechallenge with untreated CT26 cells one week later on the contralateral flank (Fig. 10G). On day 14 post-challenge, mice vaccinated with $Cu(DDC)_2$-treated cells showed a 72 % reduction in tumor volume relative to controls (Fig. 10H). Tumor-free survival reached 63 % in the vaccinated group, compared to 10 % in controls (Fig. 10I), indicating that $Cu(DDC)_2$ treatment elicits a protective, immune-mediated anti-tumor response consistent with ICD.

4. Discussion

Disulfiram is rapidly converted to DDC following oral administration, and DDC is further metabolized to diethylthiomethylcarbamate (Me-DTC), the active ALDH1 inhibitor used in alcohol dependence treatment (Mays et al., 1995). The anticancer activity of disulfiram arises when DDC binds Cu to form $Cu(DDC)_2$. Although copper levels are often elevated in the plasma and tumors of cancer patients, most circulating copper is tightly bound to carrier proteins such as ceruloplasmin and albumin, limiting the availability of free Cu^{2+} for complexation with DDC (Linder, 2016). Attempts to administer DDC intravenously have shown rapid clearance, with a terminal half-life of 3–6 min following a 4-hour infusion in humans (Awni et al., 1994). Clinical trials co-administering disulfiram with copper salts have produced mixed results, likely due to inefficient in vivo formation of $Cu(DDC)_2$, which is unlikely to reach active concentrations in tumors, and dose-limiting systemic toxicity (Dufour et al., 1993). These challenges highlight the need for direct $Cu(DDC)_2$ delivery to better control copper bioavailability and improve the therapeutic index.

The liposomal $Cu(DDC)_2$ formulation described in this study improves upon a previously developed preparation by our group that contained encapsulated copper (Wehbe et al., 2016). This new formulation is based on the sequential addition of DDC and $CuSO_4$ and the subsequent formation of $Cu(DDC)_2$ inside liposomes. The formation of $Cu(DDC)_2$ inside liposomes was unexpected since it is known that $Cu(DDC)_2$ is an insoluble precipitate. Internal and external buffer conditions were optimized, and a pH of 7.5 was determined to be optimal. The formulation retained stable size and polydispersity over 6 month storage at 4 °C, without requiring cryoprotective additives. $Cu(DDC)_2$ could not be formed or incorporated into liposomes at an external pH of 3.5, likely to due to protonation of the copper-binding thiol groups and/or decomposition of DDC (Martin, 1953; Cui et al., 2019). When using pH 7.5 external buffers, there was a significant increase in $Cu(DDC)_2$-to-lipid molar ratios compared to pH 3.5. However, at molar ratios exceeding 0.1, the formulation became difficult to filter, likely due to precipitation of $Cu(DDC)_2$ outside the liposomes.

The use of liposomes allows for a controlled analysis of copper movement across lipid bilayers. As shown (see Figs. 4 and 5), increasing copper concentrations beyond the 2:1 DDC:Cu stoichiometry did not increase $Cu(DDC)_2$ formation, but did lead to a threefold increase in liposome-associated copper. This indicates that DDC is capable of driving directional copper transport from the exterior of the liposome into the liposomal interior. Given the well-established increase in cytotoxicity observed when DDC is combined with Cu, these findings may reflect not only the activity of $Cu(DDC)_2$ itself but also the broader potential of copper transport mediated by DDC to induce copper-mediated cell death (Srikoon et al., 2013; Tsvetkov et al., 2019).

Copper accumulation and dysregulation have been linked to a range of tumor types, including breast and colon cancer, where elevated copper levels correlate with tumor progression and stage (Kannappan et al., 2021; Gupta et al., 1993; Sharma et al., 1994). This copper-dependent cell growth and proliferation, or cuproplasia, can be targeted with copper-selective chelators or with copper ionophores that increase intracellular copper levels and mediate cell death through accumulation of reactive oxygen species (ROS) in the process referred to as cuproptosis (Baldari et al., 2020; Ge et al., 2022). The role of copper and/or $Cu(DDC)_2$ in mediating anticancer effects may not be so simple and may involve the activation of immune responses. The immunomodulatory properties of DDC were first described by Renoux and colleagues, who found a stimulatory effect involving the activation of CD4 + T-cells, natural killer cells (NK) cells, and intraperitoneal cancer (Florentin et al., 1989; Chung et al., 1985; Renoux and Mrelmljgpbjm-labfoja, 1983). Recent reports have also indicated that disulfiram targets tumour-associated macrophages while increasing PD-L1 expression in cancer (Terashima et al., 2020; Zhou et al., 2019; Zheng et al., 2021). It has been shown that both disulfiram and copper individually inhibit PARP and promote PD-L1 expression, whereas the combination of disulfiram with PD-1 inhibition could produce powerful antitumour effects (Zhou et al., 2019; Zheng et al., 2021; Schwerdtle et al., 2007).

In this context, the studies here assessed the hallmark features of immunogenic cell death (ICD), including increased surface calreticulin, ATP release, and HMGB1 secretion (Sun et al., 2020; You et al., 2019), specifically in CT26 cells treated with the Cu + DDC combination. Recent reports have provided evidence of DAMP activation after treatment with disulfiram or $Cu(DDC)_2$ (Gao et al., 2022; Wang et al., 2024), and to assess whether these molecular hallmarks translated to functional antitumor immunity, we performed a prophylactic tumor vaccination assay using $Cu(DDC)_2$-treated CT26 cells. Vaccinated mice demonstrated delayed tumor growth and improved tumor-free survival upon rechallenge, supporting the ability of $Cu(DDC)_2$ to induce ICD in this setting. The induction of ICD is increasingly recognized as a key feature of certain chemotherapies, such as anthracyclines and oxaliplatin, and may also underlie the abscopal effect observed with radiation therapy (Galluzzi et al., 2020; Craig et al., 2021). These therapies convert immunologically "cold" tumors into "hot" tumors, enhancing response to immune checkpoint inhibition (ICI). Clinical trials have demonstrated

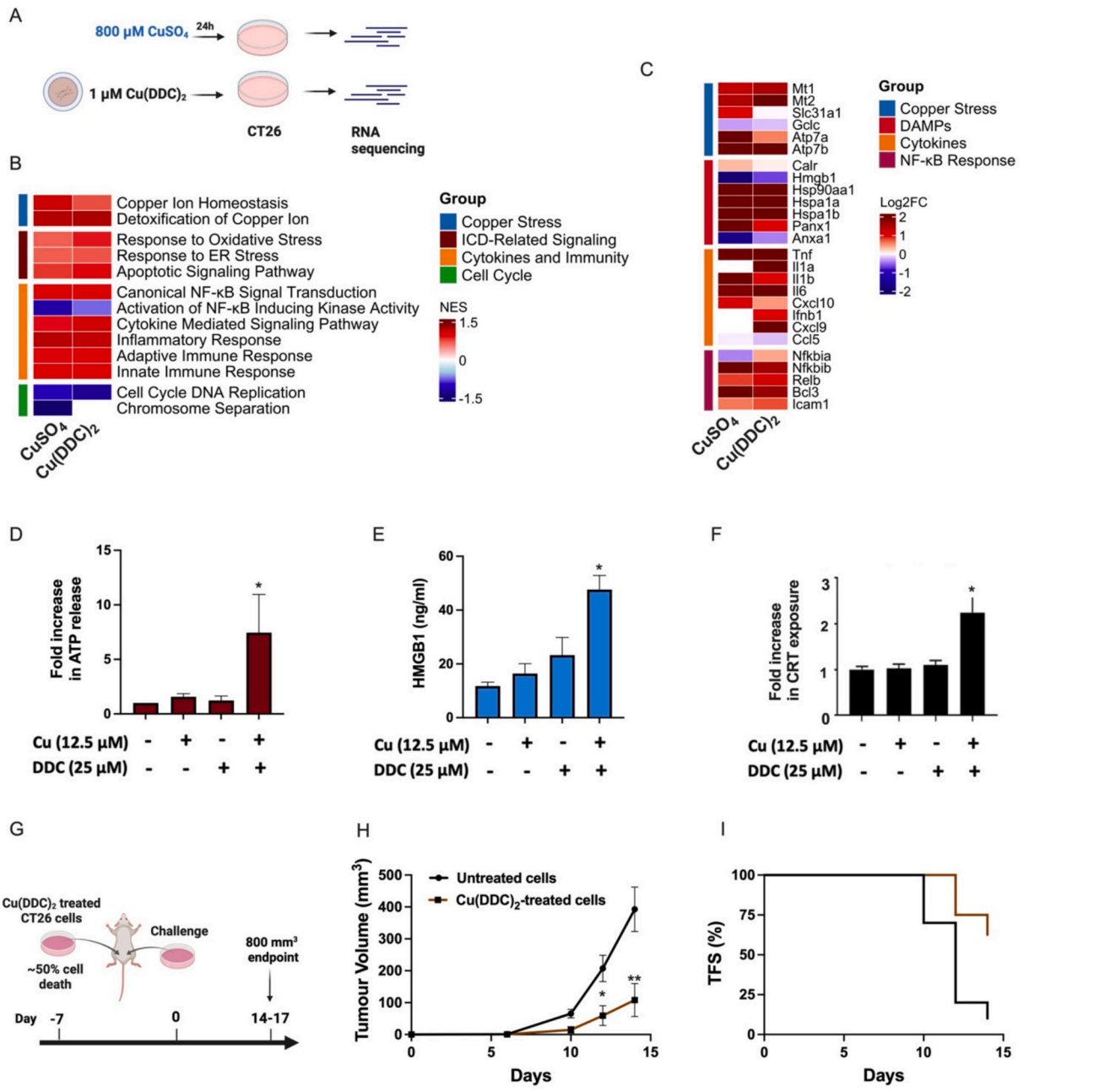

Fig. 10. $Cu(DDC)_2$ activates ICD-associated transcriptional pathways and triggers DAMP release in vitro, leading to protection in a tumor vaccination model. (A) Schematic overview of the in vitro RNA-seq experimental design. CT26 cells were treated with $CuSO_4$ (800 µM) or $Cu(DDC)_2$ (1 µM) for 24 h prior to transcriptomic analysis. (B) GSEA heatmap showing normalized enrichment scores (NES) for selected GO pathways related to copper stress, ICD, immune signaling, and cell cycle in Cu- or $Cu(DDC)_2$-treated cells. (C) Heatmap of differentially expressed genes (log_2 fold change) involved in copper stress, DAMP signaling, cytokine responses, and NF-kB response. (D–F) Independent in vitro assays confirming DAMP induction after 24 h treatment with Cu (12.5 µM), DDC (25 µM), or the combination. Extracellular ATP (D) was measured using CellTiter-Glo 2.0; HMGB1 release (E) by ELISA; and calreticulin exposure (F) by immunofluorescence. (G) Schematic of the prophylactic tumor vaccination model. CT26 cells were treated with $Cu(DDC)_2$ for 24 h, resulting in ~50 % cell death, and injected subcutaneously into the right flank of BALB/c mice. After 7 days, mice were rechallenged with untreated CT26 cells on the contralateral flank, and tumor growth was monitored to an endpoint of 800 mm^3. (H–I) Tumor growth (H) and tumor-free survival (I) following contralateral challenge in vaccinated vs. control mice. In vitro data are shown as mean ± SD; in vivo data as mean ± SEM. *P < 0.05; **P < 0.01.

improved outcomes when ICD-inducing agents are combined with PD-1 or PD-L1 blockade (Aurelius et al., 2019; Antonia et al., 2018; Voorwerk et al., 2019), with a recent trial in triple-negative breast cancer reporting that doxorubicin was able to effectively prime tumours ICI (Voorwerk et al., 2019). Disulfiram has also been shown to enhance antitumor responses in mice when combined with PD-1 inhibition (Galluzzi et al., 2020). It is our contention that the novel formulation of $Cu(DDC)_2$ developed here may be ideal for use in combination with ICI, likely through its ICD-inducing properties. In light of these findings, we propose that the Cu-o $Cu(DDC)_2$ formulation described here may serve as an effective immune priming agent in future combination approaches.

In addition to tumor cell-directed effects, $Cu(DDC)_2$ may also act on immune cell populations. Disulfiram and its metabolites have been reported to influence lymphoid and myeloid subsets in vivo (Huang et al., 2024), and the liposomal formulation's accumulation in organs rich in immune cells such as the liver and spleen may amplify these effects.

Although this study did not assess immune cells directly, ongoing work in syngeneic models is exploring these interactions in the context of immune-activating agents. The therapeutic activity observed in the MDA-MB-231 model suggests that $Cu(DDC)_2$ can exert effects independent of systemic immunity through direct tumor accumulation, and future studies will examine these biodistribution properties in models with differing immune contexts. Meanwhile, in the context of potential immunosuppression of other ICD-inducing agents (e.g., bortezomib) (Pellom et al., 2015), transcriptional analyses in CT26 cells provide preliminary support for both direct and systemic immune involvement, and further analysis of infiltrates and cytokine profiles will clarify the impact of $Cu(DDC)_2$ on the tumor microenvironment across models. These findings support a model in which $Cu(DDC)_2$ mediates both tumor-intrinsic and immune-modulating actions.

While this version of the formulation was designed primarily for mechanistic evaluation, its structure is readily suitable for therapeutic development. It enables precise control over copper delivery and elicits hallmark features of ICD, including DAMP release, transcriptional activation of stress responses, and functional immune memory. These properties, along with its compatibility with scalable production, offer a strong foundation for optimization. Future studies are focused on enhancing $Cu(DDC)_2$ loading into liposomes following administration, through further optimization of lipid composition and buffer conditions, including the incorporation of PEGylated and other circulation-prolonging systems. Recent advances in stimuli-responsive liposomal delivery—such as pH-, redox-, light-, and thermo-sensitive formulations—offer promising opportunities for site-specific drug release. As well, chemical modification of DDC may improve its lipophilicity and copper-binding properties, offering functional advantages for formulation and delivery (Xing et al., 2019). These strategies are readily adaptable to the current formulation and are under evaluation in tumor models grown in immune competent mice, particularly in combination with immune checkpoint inhibitors. Given the formulation's ability to engage both innate and adaptive immune pathways, this platform may offer a rational approach to integrating copper-based therapies with immunotherapy, especially in contexts where immune activation must be precisely modulated to maximize efficacy while limiting toxicity.

5. Conclusions

The current study describes a novel formulation of $Cu(DDC)_2$ that is suitable for *in vivo* use and capable of activating the immune system to reduce tumor burden through an immunogenic cell death (ICD) mechanism. In addition to confirming that DDC can function as a copper ionophore by transporting copper across lipid bilayers, this work establishes a foundation for exploring copper-based immunotherapies. Whether the observed effects are driven primarily by $Cu(DDC)_2$ itself or by DDC-mediated copper accumulation remains to be clarified, but the induction of functional antitumor immunity supports its potential in combination with immune checkpoint inhibition. Continued development of this platform could enable targeted copper delivery strategies that pair immune activation to enhance treatment outcomes.

CRediT authorship contribution statement

Devon Heroux: Writing – original draft, Writing – review & editing, Methodology, Investigation, Formal analysis, Conceptualization, Validation, Visualization. **Ada W.Y. Leung:** Writing – review & editing, Methodology, Investigation, Formal analysis, Conceptualization. **Roger Gilabert-Oriol:** Methodology, Investigation, Formal analysis, Conceptualization. **Jayesh Kulkarni:** Visualization, Software, Methodology, Investigation, Formal analysis, Data curation. **Malathi Anantha:** Validation, Methodology, Investigation. **Pieter R. Cullis:** Resources, Methodology. **Marcel B. Bally:** Writing – review & editing, Supervision, Resources, Funding acquisition, Conceptualization.

Funding

This research was funded by grants from the Canadian Institutes of Health Research (153132), Canadian Cancer Society (705290), and NanoMedicines Innovation Network (DRG 03190). A. Leung received financial support from the CIHR and the University of British Columbia through the Mitacs Elevate Fellowship. We would also like to thank the BC Cancer Foundation for their support of all the research done in our labs at the BC Cancer Research Institution.

Marcel Bally reports financial support was provided by Canadian Institutes of Health Research. Marcel Bally reports financial support was provided by Canadian Cancer Society. Marcel Bally reports financial support was provided by NanoMedicines Innovation Network. Ada Leung reports financial support was provided by Mitacs Canada. Copper-containing liposomal formulations were patented by BC Cancer and the patents were licensed to Cuprous Pharmaceuticals. Cuprous has now abandoned these patents and Cuprous is not currently developing formulations of Cu(DDC)2 for therapeutic use. The authors, therefore, have no conflicts of interest to declare. If there are other authors, they declare that they have no known competing financial interests or personal relationships that could have appeared to influence the work reported in this paper.

Declaration of competing interest

The authors declare the following financial interests/personal relationships which may be considered as potential competing interests: Marcel Bally reports financial support was provided by Canadian Institutes of Health Research. Marcel Bally reports financial support was provided by Canadian Cancer Society. Marcel Bally reports financial support was provided by NanoMedicines Innovation Network. Ada Leung reports financial support was provided by Mitacs Canada. Copper-containing liposomal formulations were patented by BC Cancer and the patents were licensed to Cuprous Pharmaceuticals. Cuprous has now abandoned these patents and Cuprous is not currently developing formulations of Cu(DDC)2 for therapeutic use. The authors, therefore, have no conflicts of interest to declare. If there are other authors, they declare that they have no known competing financial interests or personal relationships that could have appeared to influence the work reported in this paper.

Acknowledgement

The authors would like to thank the Investigational Drug Program (PharmaCore) at the BC Cancer Research Institution for their technical contribution to our *in vivo* studies, and Norman Chow for his technical assistance. Figures created with BioRender.com.

Appendix A. Supplementary data

Supplementary data to this article can be found online at https://doi.org/10.1016/j.ijpharm.2025.126010.

Data availability

Data will be made available on request.

References

Allensworth, J.L., Evans, M.K., Bertucci, F., Aldrich, A.J., Festa, R.A., Finetti, P., et al., 2015. Disulfiram (DSF) acts as a copper ionophore to induce copper-dependent oxidative stress and mediate anti-tumor efficacy in inflammatory breast cancer. Mol. Oncol. 9, 1155–1168. https://doi.org/10.1016/j.molonc.2015.02.007.

Antonia, S.J., Villegas, A., Daniel, D., Vicente, D., Murakami, S., Hui, R., et al., 2018. Overall survival with durvalumab after chemoradiotherapy in stage III NSCLC. N. Engl. J. Med. https://doi.org/10.1056/NEJMoa1809697.

Aurelius, J., Möllgård, L., Kiffin, R., Ewald Sander, F., Nilsson, S., Thorén, F.B., et al., 2019. Anthracycline-based consolidation may determine outcome of post-

consolidation immunotherapy in AML. Leuk. Lymphoma. https://doi.org/10.1080/10428194.2019.1599110.
Awni, W.M., Hoff, J.V., Shapiro, B.E., Halstenson, C.E., 1994. A dose-ranging pharmacokinetics study of sodium diethyldithiocarbamate in normal healthy volunteers. J. Clin. Pharmacol. 34, 1183–1190. https://doi.org/10.1002/j.1552-4604.1994.tb04730.x.
B, M., Phase II Trial of Disulfiram With Copper in Metastatic Breast Cancer (DISC). 2017-Ongoing: ClinicalTrials.gov Identifier: NCT03323346. n.d.
Baldari, S., Di Rocco, G., Toietta, G., 2020. Current biomedical use of copper chelation therapy. Int. J. Mol. Sci. 21, 1069. https://doi.org/10.3390/ijms21031069.
Caetano-Silva, M.E., Rund, L.A., Vailati-Riboni, M., Pacheco, M.T.B., Johnson, R.W., 2021. Copper-binding peptides attenuate microglia inflammation through suppression of NF-kB pathway. Mol. Nutr. Food Res. 65, e2100153. https://doi.org/10.1002/mnfr.202100153.
Chung, V., Florentin, I., Renoux, G., 1985. Effect of imuthiol administration to normal or immunodeficient mice on IL 1 and IL2 production and immune responses regulated by these mediators. J. Immunopharmacol. 7, 335.
Craig, D.J., Nanavaty, N.S., Devanaboyina, M., Stanbery, L., Hamouda, D., Edelman, G., et al., 2021. The abscopal effect of radiation therapy. Future Oncol. 17, 1683–1694. https://doi.org/10.2217/fon-2020-0994.
Cui, B., Wang, X., Zhao, Q., Liu, W., 2019. Study on the degradation of sodium diethyldithiocarbamate (DDTC) in artificially prepared beneficiation wastewater with sodium hypochlorite. J. Chem. 2019, 7038015. https://doi.org/10.1155/2019/7038015.
Cvek, B., Milacic, V., Taraba, J., Dou, Q.P., 2008. Ni(II), Cu(II), and Zn(II) diethyldithiocarbamate complexes show various activities against the proteasome in breast cancer cells. J. Med. Chem. https://doi.org/10.1021/jm8007807.
Dufour, P., Lang, J.M., Giron, C., Duclos, B., Haehnel, P., Jaeck, D., et al., 1993. Sodium ditiocarb as adjuvant immunotherapy for high risk breast cancer: a randomized study. Biotherapy. https://doi.org/10.1007/BF01877380.
Fasehee, H., Dinarvand, R., Ghavamzadeh, A., Esfandyari-Manesh, M., Moradian, H., Faghihi, S., et al., 2016. Delivery of disulfiram into breast cancer cells using folate-receptor-targeted PLGA-PEG nanoparticles: In vitro and in vivo investigations. J. Nanobiotechnol. https://doi.org/10.1186/s12951-016-0183-z.
Florentin, I., Vér, C., Renoux, M., Gér, R., 1989. Imuthiol influences on cytotoxic T cells and NK activity in +/+ and athymic nude BALB/c mice. Immunopharmacol. Immunotoxicol. 11, 645–655. https://doi.org/10.3109/08923978909005392.
Galluzzi, L., Vitale, I., Warren, S., Adjemian, S., Agostinis, P., Martinez, A.B., et al., 2020. Consensus guidelines for the definition, detection and interpretation of immunogenic cell death. J. Immunother. Cancer. https://doi.org/10.1136/jitc-2019-000337.
Gao, X., Huang, H., Pan, C., Mei, Z., Yin, S., Zhou, L., et al., 2022. Disulfiram/copper induces immunogenic cell death and enhances CD47 blockade in hepatocellular carcinoma. Cancers (Basel) 14. https://doi.org/10.3390/cancers14194715.
Ge, E.J., Bush, A.I., Casini, A., Cobine, P.A., Cross, J.R., DeNicola, G.M., et al., 2022. Connecting copper and cancer: from transition metal signalling to metalloplasia. Nat. Rev. Cancer 22, 102–113. https://doi.org/10.1038/s41568-021-00417-2.
Gupta, S.K., Shukla, V.K., Vaidya, M.P., Roy, S.K., Gupta, S., 1993. Serum and tissue trace elements in colorectal cancer. J. Surg. Oncol. 52, 172–175. https://doi.org/10.1002/jso.2930520311.
Helsel, M.E., Franz, K.J., 2015. Pharmacological activity of metal binding agents that alter copper bioavailability. Dalton Trans. https://doi.org/10.1039/c5dt00634a.
Hordyjewska, A., Popiołek, Ł., Kocot, J., 2014. The many "faces" of copper in medicine and treatment. Biometals : Int. J. Role Metal Ions Biol., Biochem. Med. 27 (4), 611–621 n.d.
Huang, D., Yao, Y., Lou, Y., Kou, L., Yao, Q., Chen, R., 2024. Disulfiram and cancer immunotherapy: advanced nano-delivery systems and potential therapeutic strategies. Int. J. Pharm. X 8, 100307. https://doi.org/10.1016/j.ijpx.2024.100307.
Huo, Q., et al., 2017. pH-triggered surface charge-switchable polymer micelles for the co-delivery of paclitaxel/disulfiram and overcoming multidrug resistance in cancer. Int. J. Nanomed. 12, 8631–8647 n.d.
Kang, X., Wang, J., Huang, C.-H., Wibowo, F.S., Amin, R., Chen, P., et al., 2023. Diethyldithiocarbamate copper nanoparticle overcomes resistance in cancer therapy without inhibiting P-glycoprotein. Nanomed. Nanotechnol. Biol. Med. 47, 102620. https://doi.org/10.1016/j.nano.2022.102620.
Kannappan, V., Ali, M., Small, B., Rajendran, G., Elzhenni, S., Taj, H., et al., 2021. Recent advances in repurposing disulfiram and disulfiram derivatives as copper-dependent anticancer agents. Front. Mol. Biosci. 8. https://doi.org/10.3389/fmolb.2021.741316.
Lichtnekert, J., Kawakami, T., Parks, W.C., Duffield, J.S., 2013. Changes in macrophage phenotype as the immune response evolves. Curr. Opin. Pharmacol. https://doi.org/10.1016/j.coph.2013.05.013.
Linder, M.C., 2016. Ceruloplasmin and other copper binding components of blood plasma and their functions: an update. Metallomics 8, 887–905. https://doi.org/10.1039/c6mt00103c.
Liu, P., Wang, Z., Brown, S., Kannappan, V., Tawari, P.E., Jiang, W., et al., 2014. Liposome encapsulated disulfiram inhibits NFκB pathway and targets breast cancer stem cells in vitro and in vivo. Oncotarget. https://doi.org/10.18632/oncotarget.2166.
Loo, T.W., Clarke, D.M., 2000. Blockage of drug resistance in vitro by disulfiram, a drug used to treat alcoholism. J. Natl Cancer Inst. https://doi.org/10.1093/jnci/92.11.898.
Lövborg, H., Öberg, F., Rickardson, L., Gullbo, J., Nygren, P., Larsson, R., 2006. Inhibition of proteasome activity, nuclear factor-KB translocation and cell survival by the antialcoholism drug disulfiram. Int. J. Cancer. https://doi.org/10.1002/ijc.21534.
Mardiak J, M.M., n.d. Disulfiram and cisplatin in refractory TGCTs. (DISGCT). 2019-Ongoing (ClinicalTrials.gov Identifier: NCT03950830).
Martin, A.E., 1953. Instability of diethyldithiocarbamic acid at low pH. Anal. Chem. 25, 1260–1261. https://doi.org/10.1021/ac60080a035.
Mays, D.C., Nelson, A.N., Fauq, A.H., Shriver, Z.H., Veverka, K.A., Naylor, S., et al., 1995. S-methyl N,N-diethylthiocarbamate sulfone, a potential metabolite of disulfiram and potent inhibitor of low Km mitochondrial aldehyde dehydrogenase. Biochem. Pharmacol. 49, 693–700. https://doi.org/10.1016/0006-2952(94)00504-F.
McElwee, M.K., Song, M.O., Freedman, J.H., 2009. Copper activation of NF-kappaB signaling in HepG2 cells. J. Mol. Biol. 393, 1013–1021. https://doi.org/10.1016/j.jmb.2009.08.077.
Nechushtan, H., Hamamreh, Y., Nidal, S., Gotfried, M., Baron, A., Shalev, Y.I., et al., 2015. A phase IIb trial assessing the addition of disulfiram to chemotherapy for the treatment of metastatic non-small cell lung cancer. Oncologist. https://doi.org/10.1634/theoncologist.2014-0424.
Otoniel, D., Sant'AnaLuciene, S., JesuinoRicardo, J., CassellaMarcelo, S., CarvalhoRicardo, E., Santelli, 2003. Solid phase extraction of Cu(II) as diethyldithiocarbamate (DDTC) complex by polyurethane foam. J. Braz. Chem. So. 14, 728–733.
Paun, R.A., Dumut, D.C., Centorame, A., Thuraisingam, T., Hajduch, M., Mistrik, M., et al., 2022. One-step synthesis of nanoliposomal copper diethyldithiocarbamate and its assessment for cancer therapy. Pharmaceutics 14, 640. https://doi.org/10.3390/pharmaceutics14030640.
Pellom, S.T., Dudimah, D.F., Thounaojam, M.C., Sayers, T.J., Shanker, A., 2015. Modulatory effects of bortezomib on host immune cell functions. Immunotherapy 7, 1011–1022. https://doi.org/10.2217/imt.15.66.
Percie du Sert, N., Ahluwalia, A., Alam, S., Avey, M.T., Baker, M., Browne, W.J., et al., 2020. Reporting animal research: explanation and elaboration for the ARRIVE guidelines 2.0. PLoS Biol. 18, e3000411. https://doi.org/10.1371/journal.pbio.3000411.
Renoux, G., MRELMLJGPBJMLABFOJA, et al., 1983. Sodium diethyldithiocarbamate (imuthiol) and cancer. Adv. Exp. Med. Biol. 166, 223–239.
Schirmer, H.K., Scott, W.W., 1966. Disulfiram and tumor inhibition. Trans. Am. Assoc. Genitourin. Surg.
Schwerdtle, T., Hamann, I., Jahnke, G., Walter, I., Richter, C., Parsons, J.L., et al., 2007. Impact of copper on the induction and repair of oxidative DNA damage, poly(ADP-ribosyl)ation and PARP-1 activity. Mol. Nutr. Food Res. 51, 201–210. https://doi.org/10.1002/mnfr.200600107.
Sharma, K., Mittal, D.K., Kesarwani, R.C., Chowdhery, K.VP., 1994. Diagnostic and prognostic significance of serum and tissue trace elements in breast malignancy. Indian J. Med. Sci. 48 (10), 227–232.
Skrott, Z., Mistrik, M., Andersen, K.K., Friis, S., Majera, D., Gursky, J., et al., 2017. Alcohol-abuse drug disulfiram targets cancer via p97 segregase adaptor NPL4. Nature. https://doi.org/10.1038/nature25016.
Srikoon, P., Kariya, R., Kudo, E., Goto, H., Vaeteewoottacharn, K., Taura, M., Wongkham, S.O.S., 2013. Diethyldithiocarbamate suppresses an NF-kappaB dependent metastatic pathway in cholangiocarcinoma cells. Asian Pac. J. Cancer Prev. 14 (7), 4441–4446.
Sun, T., Yang, W., Toprani, S.M., Guo, W., He, L., DeLeo, A.B., et al., 2020. Induction of immunogenic cell death in radiation-resistant breast cancer stem cells by repurposing anti-alcoholism drug disulfiram. Cell Commun. Signal 18, 36. https://doi.org/10.1186/s12964-019-0507-3.
Terashima, Y., Toda, E., Itakura, M., Otsuji, M., Yoshinaga, S., Okumura, K., et al., 2020. Targeting FROUNT with disulfiram suppresses macrophage accumulation and its tumor-promoting properties. Nat. Commun. 11, 609. https://doi.org/10.1038/s41467-020-14338-5.
Tsvetkov, P., Detappe, A., Cai, K., Keys, H.R., Brune, Z., Ying, W., et al., 2019. Mitochondrial metabolism promotes adaptation to proteotoxic stress. Nat. Chem. Biol. 15, 681–689. https://doi.org/10.1038/s41589-019-0291-9.
Viola-Rhenals, M., et al., 2018. Recent advances in antabuse (disulfiram): the importance of its metal-binding ability to its anticancer activity. Curr. Med. Chem. 25 (4), 506–524 n.d.
Voorwerk, L., Slagter, M., Horlings, H.M., Sikorska, K., van de Vijver, K.K., de Maaker, M., et al., 2019. Immune induction strategies in metastatic triple-negative breast cancer to enhance the sensitivity to PD-1 blockade: the TONIC trial. Nat. Med. https://doi.org/10.1038/s41591-019-0432-4.
Wang, R., Song, W., Zhu, J., Shao, X., Yang, C., Xiong, W., et al., 2024. Biomimetic nano-chelate diethyldithiocarbamate Cu/Fe for enhanced metalloimmunity and ferroptosis activation in glioma therapy. J. Control. Release 368, 84–96. https://doi.org/10.1016/j.jconrel.2024.02.004.
Wattenberg, L.W., 1975. Inhibition of dimethylhydrazine induced neoplasia of the large intestine by disulfiram. J. Natl Cancer Inst. https://doi.org/10.1093/jnci/54.4.1005.
Wehbe, M., Anantha, M., Backstrom, I., Leung, A., Chen, K., Malhotra, A., et al., 2016. Nanoscale reaction vessels designed for synthesis of copper-drug complexes suitable for preclinical development. PLoS One 11, e0153416. https://doi.org/10.1371/journal.pone.0153416.
Wehbe, M., Anantha, M., Shi, M., Leung, A.W.Y., Dragowska, W.H., Sanche, L., et al., 2017. Development and optimization of an injectable formulation of copper diethyldithiocarbamate, an active anticancer agent. Int. J. Nanomed. https://doi.org/10.2147/IJN.S137347.
Xing, J., Zhang, X., Wang, Z., Zhang, H., Chen, P., Zhou, G., et al., 2019. Novel lipophilic SN38 prodrug forming stable liposomes for colorectal carcinoma therapy. Int. J. Nanomed. 14, 5201–5213. https://doi.org/10.2147/IJN.S204965.
You, S.-Y., Rui, W., Chen, S.-T., Chen, H.-C., Liu, X.-W., Huang, J., et al., 2019. Process of immunogenic cell death caused by disulfiram as the anti-colorectal cancer candidate.

Biochem. Biophys. Res. Commun. 513, 891–897. https://doi.org/10.1016/j.bbrc.2019.03.192.
Zheng, X., Liu, Z., Mi, M., Wen, Q., Zhang, L., Yin, M., et al., 2021. Disulfiram improves the anti-PD-1 therapy efficacy by regulating PD-L1 expression via epigenetically reactivation of IRF7 in triple negative. Breast Cancer 11. https://doi.org/10.3389/fonc.2021.734853.
Zheng, X., Liu, Z., Mi, M., Wen, Q., Wu, G., Zhang, L., 2021. Disulfiram improves the anti-PD-1 therapy efficacy by regulating PD-L1 expression via epigenetically reactivation of IRF7 in triple negative breast cancer. Front. Oncol. 11, 734853. https://doi.org/10.3389/fonc.2021.734853.
Zhou, B., Guo, L., Zhang, B., Liu, S., Zhang, K., Yan, J., et al., 2019. Disulfiram combined with copper induces immunosuppression via PD-L1 stabilization in hepatocellular carcinoma. Am. J. Cancer Res. 9, 2442–2455.